Quantification of thermodynamic properties for vaporisation reactions above solid Ga2O3 and In2O3 by Knudsen Effusion Mass Spectrometry

Author(s):
Bischof, Lukas; Sossi, Paolo A.; Sergeev, Dmitry; Müller, Michael; Schmidt, Max W.

Publication date:
2023-03

Permanent link:
https://doi.org/10.3929/ethz-b-000592445

Originally published in:
Calphad 80, https://doi.org/10.1016/j.calphad.2022.102507

Funding acknowledgement:
180025 - Experimental and stable isotope constraints on the accretion and differentiation of the terrestrial planets (SNF)

CALPHAD: Computer Coupling of Phase Diagrams and Thermochemistry 80 (2023) 102507

Contents lists available at ScienceDirect

Calphad

journal homepage: www.elsevier.com/locate/calphad

Quantification of thermodynamic properties for vaporisation reactions above solid Ga_2O_3 and In_2O_3 by Knudsen Effusion Mass Spectrometry

Lukas Bischof [a,*], Paolo A. Sossi [a], Dmitry Sergeev [b], Michael Müller [b], Max W. Schmidt [a]

[a] Institute of Geochemistry and Petrology, ETH Zürich, CH-8092, Zürich, Switzerland
[b] IEK-2, Forschungszentrum Jülich, Jülich, Germany

A B S T R A C T

Even though Ga_2O_3 and In_2O_3 are broadly used as semi-conductors, thermodynamic data for their vaporisation reactions exhibit a large spread. Therefore, the vaporisation behaviour of solid Ga_2O_3 and In_2O_3 was determined by means of Knudsen Effusion Mass Spectrometry (KEMS). Ga_2O_3 and In_2O_3 were studied in an iridium Knudsen cell and heated over a temperature range of 1200–1750 K in order to identify the species present in the vapour phase, and determine their partial pressures. We find that M_2O (where M = Ga or In) is the most abundant gas species above the solid oxide, followed by M and MO, in accord with tabulated data. Following the calculation of partial pressures and equilibrium constants, we propose $\Delta_f H^{o}_{298,\,3rd}(Ga_2O(g)) = -68966 \pm 7442$ Jmol^{-1} and $\Delta_f H^{o}_{298,\,3rd}(In_2O(g)) = -22245 \pm 964$ Jmol^{-1} from the 3rd law method. Deviations in $\Delta_f H^{o}_{298,\,3rd}(i)$ relative to literature KEMS measurements are generally within ~2% relative, and can be ascribed to the use of different ionisation cross sections, Knudsen cell material, temperature calibrations, as well as tabulated Gibbs energy functions. However, comparison with *ab initio* studies suggests the data reported in this work is more accurate than in previous studies, given that the $\Delta_f H^{o}_{298,\,3rd}(InO(g)) = 157744 \pm 3681$ Jmol^{-1} deviates by only ~0.2% from the theoretical value.

1. Introduction

Gallium oxide (Ga_2O_3) as well as Indium oxide (In_2O_3) are polymorphous sesquioxides in which the metal is trivalent. Ga_2O_3 is an insulator with a wide band gap at room temperature (4.9 eV); the widest among transparent conducting oxides [1–3]. Ga_2O_3 is applied to the preparation of gas sensors, optoelectronic devices, luminescent materials and catalysts in multiple gas and liquid phase chemical reactions. There are five different structures (α, β, γ, δ, ε) known for Ga_2O_3, differing not only in crystal space group, but also in coordination number of Ga^{III} [3,4]. Among the five, the only stable form throughout the whole temperature range to the melting point of 2013 K is β-Ga_2O_3, all other polymorphs convert into β-Ga_2O_3 above 1143 K [3,4]. The β-Ga_2O_3 polymorph crystallises in the monoclinic space group $C2/m$, in which oxygen forms a distorted cubic close-packing and Ga^{III} occupies the octahedral- and tetrahedral sites [3,5].

Pure In_2O_3 is applied as gas sensor and semi-conductor, inter alia. However, In_2O_3 is most widely used in its tin-doped form indium-tin-oxide (ITO), *e.g.* in transparent contacts for flat panel displays and solar cells, in transparent current spreading layers in surface light emitting diodes, in infrared reflective and electrochromic windows and in cladding layers for InGaN-based lasers [2]. The compound In_2O_3 has an α- and β-polymorph. The α-In_2O_3 polymorph has a body centred cubic bixbyite (Mn_2O_3) structure (space group $Ia\bar{3}$) derived from a face centred cubic fluorite structure with 1/4 of the oxygens removed. In this lattice, In occupies two non-equivalent positions and is surrounded by oxygens in either octahedral or trigonal prismatic coordination. At 1273 K, 3.8 GPa, α-In_2O_3 transforms into β-In_2O_3, which crystallises in a rhombohedral structure analogous to α-Al_2O_3 (corundum, space group $R\bar{3}c$) before reaching its melting point of 2183 K [2,6,7].

Despite the well-defined structures and physical properties of the group XIII sesquioxides, there is a lack of thermodynamic data, namely equilibrium constants, enthalpies and entropies for the evaporation reactions of the solid metal oxides, M_2O_3(s), into M(g), MO(g) and M_2O(g). The first such study, by Shchukarev et al. [8], investigated the evaporation of Ga_2O_3(s) and In_2O_3(s) and determined partial pressures for different species, p_i, mass-spectrometrically with an alumina (Al_2O_3) Knudsen effusion cell between 1373 and 1973 K. They detected M^+, M_2^+, MO^+, M_2O^+, M_2O^{2+} as well as O_2^+ above the heated metal oxides. However, these authors *a priori* assumed a $p(M_2O)$:$p(M)$ ratio of 1:0.01 over the entire temperature range, casting doubt over the reported p_i values. Nevertheless, the fact that lower temperatures are required to reach similar partial pressures, $p(In_2O(g))$ reaches 12 Pa at 1631 K which exceeds $p(Ga_2O(g))$ at 1728 K, 4 Pa, means that In_2O_3 is more volatile than Ga_2O_3.

* Corresponding author.
E-mail address: lukas.bischof@erdw.ethz.ch (L. Bischof).

https://doi.org/10.1016/j.calphad.2022.102507
Received 22 July 2022; Received in revised form 10 October 2022; Accepted 19 November 2022
Available online 5 January 2023

Gomez et al. [9] studied the gaseous species produced by vaporisation of In_2O_3(s) from 1340 to 1618 K with a special focus on their ion fragmentation patterns. These authors used a Pt-crucible in an Al_2O_3 Knudsen effusion cell coupled to a mass spectrometer, and the setup included a ZrO_2-based electrochemical cell to impose an oxygen pressure, hence enabling the analysis of ion fragmentation at different $p(O_2)$. Gomez et al. [9] identified three In-bearing ions, In^+, InO^+, In_2O^+ in the gaseous phase and deduced, on the basis of their appearance potentials, that, during ionisation, In_2O fragmentation into In^+ is much more favourable than into InO^+. They measured p(In), p(InO), $p(In_2O)$ and $p(O_2)$ values similar to those obtained by Shchukarev et al. [8] at comparable temperatures. Gomez et al. [9] concluded that In_2O(g) is the most abundant species above In_2O_3(s) and that the congruent dissociative evaporation of In_2O_3(s) into In_2O(g) and O_2(g) is the thermodynamically-favoured stoichiometry. The standard enthalpy change for $In_2O_3(s) = In_2O(g) + O_2(g)$ calculated from Shchukarev et al. [8] gives $\Delta_r H^{\circ}_{298,\ 2nd} = 922253$ Jmol^{-1} and $\Delta_r H^{\circ}_{298,\ 3rd} = 873201$ Jmol^{-1} by the 2nd and 3rd-law methods, respectively, while that reported by Gomez et al. [9] is $\Delta_r H^{\circ}_{298,\ 3rd} = 895000 \pm 2000$ Jmol^{-1}.

Given the ambiguity in assigning the measured ion intensities and the contrasting thermodynamic data for Ga_2O_3 and In_2O_3, further study is warranted. This was also recognised by Smirnov et al. [10], who examined the vaporisation of In_2O_3(s) from 1400 to 1610 K by means of a quartz effusion cell. These authors emphasised the choice of cell material in minimising reaction with In_2O_3(s). In addition, In–In_2O_3 mixtures allowed them to better characterise the intensities of the fragmentation products of In_2O(g) into its daughter molecules during ionisation, thereby permitting a more accurate determination of the partial pressures of In-bearing gas species. The resulting standard enthalpy of formation of gaseous In_2O, $\Delta_f H^{\circ}_{298,\ 3rd}(In_2O)$, is -30700 ± 15900 Jmol^{-1}, $\Delta_r H^{\circ}_{298,\ 2nd} = 900300 \pm 115600$ Jmol^{-1} and $\Delta_r H^{\circ}_{298,\ 3rd} = 893100 \pm 12700$ Jmol^{-1} for the reaction $In_2O_3(s) = In_2O(g) + O_2$ (g).

Following their investigation of the vaporisation of In_2O_3(s), Smirnov et al. [11] examined vaporisation in the system In–In_2O_3 from 930 to 1210 K, using the same method (KEMS, quartz effusion cell) as described in Smirnov et al. [10]. They find that the standard enthalpy of formation of In_2O(g) from both studies are in good agreement and propose an updated value of $\Delta_f H^{\circ}_{298,\ 3rd}(In_2O) = -31300 \pm 8700$ Jmol^{-1}.

In this study, we reinvestigate p(M), p(MO) and $p(M_2O)$ between 1200 and 1750 K above Ga_2O_3 and In_2O_3. Owing to the fact that these p_i depend on $p(O_2)$, we calculate equilibrium constants K based on p_i measured here and those taken from literature in order to enable a robust comparison. Subsequently, the enthalpy $\Delta_r H^{\circ}_{T,\ 2nd}$ and entropy $\Delta_r S^{\circ}_{T,\ 2nd}$ of reaction for the average temperature of the measurement are obtained via a van't Hoff plot of K *vs.* temperature T, whereas $\Delta_r H^{\circ}_{298,\ 2nd}$, $\Delta_r H^{\circ}_{298,\ 3rd}$, $\Delta_f H^{\circ}_{298,\ 2nd}(i)$ and $\Delta_f H^{\circ}_{298,\ 3rd}(i)$ are obtained via the combination of K with Gibbs energy functions from literature referenced to 298 K, $gef^{\circ}_{298}(T)$, at T of the measurement.

All thermodynamic quantities applied within this work are summarised in Table 1.

Table 1
Summary of thermodynamic quantities applied within this work.

Quantity	Definition	Quantity	Definition
$gef^{\circ}_{298}(T)$	Gibbs energy function, referenced to 298 K, at T of the measurement and standard pressure	$\Delta_r H^{\circ}_{298,\ 2nd}$	Standard enthalpy of reaction based on 2nd-law method
$\Delta_r gef^{\circ}_{298}(T)$	Gibbs energy function of reaction, referenced to 298 K, at T of the measurement and standard pressure	$\Delta_r H^{\circ}_{298,\ 3rd}$	Standard enthalpy of reaction based on 3rd-law method
$\Delta_f H^{\circ}_{298,\ 2nd}(i)$	Standard enthalpy of formation of species i based on 2nd-law method	K	Equilibrium constant
$\Delta_f H^{\circ}_{298,\ 3rd}(i)$	Standard enthalpy of formation of species i based on 3rd -law method	p_i	Partial pressure of species i
$\Delta_r H^{\circ}_{T,\ 2nd}$	Enthalpy of reaction at standard pressure and average T of the measurement based on 2nd-law method	$\Delta_r S^{\circ}_{T,\ 2nd}$	Enthalpy of reaction at standard p and average T of the measurement based on 2nd-law method

2. Methods

2.1. Knudsen Effusion Mass Spectrometry (KEMS)

The schematic setup of the FINNIGAN MAT 271 Knudsen effusion mass spectrometer at the Forschungszentrum, Jülich used in this work is shown in Fig. 1. It can be subdivided into four main components: a Knudsen cell (KC), an electron impact ion source, a single-focusing magnetic type sector-field mass spectrometer and a collector arrangement of a Faraday cup and a multiplier [14]. The iridium KC contains the sample to be analysed and is composed of a crucible 8.5 mm high with an outer diameter of 7.8 mm and 0.2 mm wall thickness, and a lid with a 0.4 mm orifice at its centre. A tungsten container directly encases the KC, followed by three tantalum heat shields nested one inside the other. All parts have openings to enable the effusion of a molecular beam axial to the cell. The KC is heated via radiation up to temperatures of ~873 K and by electron bombardment at higher temperatures, both by means of a tungsten heating wire that is braided around the KC-bearing tungsten container [14,15]. The temperature in the Knudsen cell chamber is monitored by a $W_{97}Re_3/W_{75}Re_{25}$ thermocouple, which is part of the Knudsen cell holder that is positioned directly underneath the KC ("heating element" in Fig. 1), while the temperature at the KC is determined via a hole in the tungsten container (Fig. 1, inset) below the sample using a single wavelength IGA-12 pyrometer (LUMASENSE TECHNOLOGIES). The whole assembly is located in the Knudsen cell chamber, evacuated through a turbo molecular pump to ~10^{-6} mbar, and can be isolated through a shutter from the other mass spectrometer compartments that are constantly kept under ultrahigh vacuum (~10^{-9} mbar) by ion getter pumps. The shutter also permits distinction between sample- and background signals during the measurement by blocking the passage of the molecular beam. When open, the molecular beam effusing out of the KC passes an aperture and enters the ion source, where the ionisation of gaseous species takes place. For ionisation to occur, an electron beam is generated by an incandescent cathode (electron energy between 60 and 70 eV; emission current: 0.468 mA), which runs perpendicular to the molecular beam. The detector consists of a collector arrangement of a Faraday cup and an electron multiplier, with the former being applied for large and the latter for small amounts of ions to be analysed. Since ion-counting allows the avoidance of measurement errors by virtue of mass discrimination through the multiplier, this method is adopted for the experiments performed within the scope of this work.

Prior to sample loading, empty Knudsen cells were baked out for 12 h at 1930 K to vaporise any impurities in the system and to anneal the iridium. Approximately 40 mg of pure (>99.9%) Ga_2O_3 or In_2O_3 (*cf.* Table 3) was loaded as a fine powder and weighed together with the other components of the Knudsen cell. The KC was then placed in the Knudsen cell chamber (Fig. 1), and, when the vacuum reached ~10^{-6} mbar or better, the sample was slowly heated up to ~973 K. Mass scans from *mass* 10 to *mass* 250 were performed intermittently thereafter in order to check for the presence of vapour species above the sample. Once a sufficiently intense signal was detected (invariably either Ga^+ or In^+), the spatial position of the KC was adjusted in order to optimise the measured signal. All measurements were performed using an electron ionisation energy $E(e^-)$ of 60 eV or 70 eV at a constant electron emission $i_{(em)}$ of 0.468 mA. Each species was measured over a 1% mass window of its nominal mass, with a scan consisting of 301 steps and a counting time

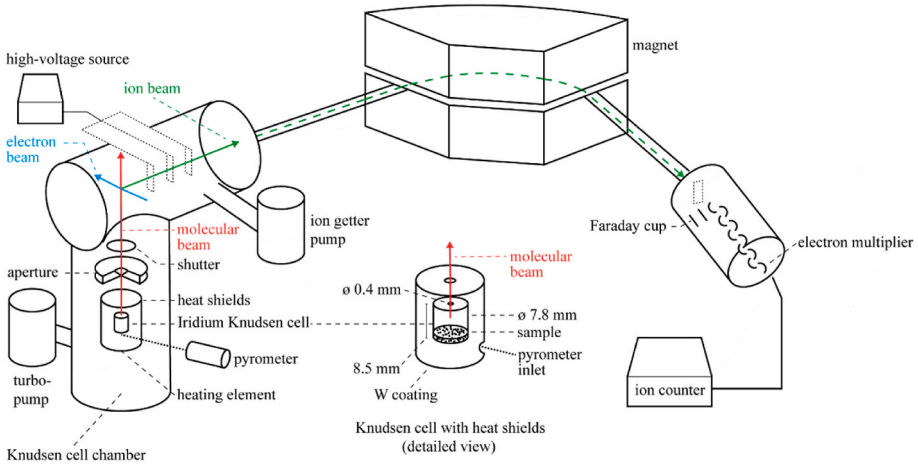

Fig. 1. Schematic view of a magnetic-sector Knudsen effusion mass spectrometer applied. Adapted from Costa et al. [12] and Dong et al. [13].

Table 2
Masses and natural abundances (if applicable) of the ions measured in this work.

Ga			In		
Species	*m/z*	Natural abundance [%]	Species	*m/z*	Natural abundance [%]
Ga^+	69	60.1	In^+	115	95.7
				113	4.3
Ga^{2+}	34.5	–	In^{2+}	57.5	–
Ga^{3+}	23	–	In^{3+}	38	–
GaO^+	85	60.0	InO^+	131	95.5
Ga_2^+	138	36.1	In_2^+	230	91.6
Ga_2O^+	156	47.9	In_2O^+	246	91.4

of 0.1 s/step. Two types of measurement series were performed; *isotherm* and *polytherm*. The isotherm pertains to the measurement of vapour speciation at a fixed temperature over a given duration, whereas the polytherm involves isotherm measurements performed at discrete temperature steps. The measured species and their respective mass-to-charge ratio (*m/z*) are listed in Table 2, the conditions for the individual measurements are summarised in Table 3.

2.2. X-ray diffraction (XRD)

Gallium and indium oxide were analysed via X-ray diffraction before and after the KEMS experiments. For this purpose, the powders were mixed under acetone in equivalent proportion with a NIST Si metal standard for peak calibration. The resulting slurry was distributed onto a low-background single-crystal quartz plate and then placed horizontally on a rotating stage. The analysis was carried out via a Bruker AXS D8 Advance X-ray diffractometer, equipped with a Lynxeye superspeed detector with a monochromatic Cu Kα_1 X-ray source ($\lambda = 1.54$ Å). The data were collected from 5 to 110° with a step size of 0.0158°, a recording time per step of 0.8 s and a divergence slit of 20 mm. Results were compared to literature data by Marezio and Remeika [16] and Åhman et al. [17] for Ga_2O_3 as well as to Nadaud et al. [18] for In_2O_3 (*cf.* section 4.1 and Appendix).

3. Theoretical framework

The size of the orifice is chosen to promote equilibrium conditions within the cell whilst maintaining molecular (rather than hydrodynamic) flow, *i.e.*, effusion through the orifice, which can be quantified according to the Knudsen number of the gas (eq. (1));

$$Kn = \frac{\lambda}{d_0} \tag{1}$$

where λ is the mean free path and d_0 the diameter of the orifice. The mean free path is given by the ideal gas law (eq. (2)):

$$\lambda = \frac{k_B T}{P} \frac{1}{\sqrt{2}\pi d^2} \tag{2}$$

where k_B is the Boltzmann constant, T absolute temperature, P total pressure and d the kinetic diameter. In practice, effusion is achieved for values of $Kn \geq 8$ ([19]; and references therein). Therefore, for our nominal measurement conditions with a 0.4 mm orifice at 1600 K and a

Table 3
Samples, their weights and measurement parameters in isotherm and polytherm runs.

Sample	Run	Initial weight [mg]	Final weight [mg]	Isotherm parameters		Polytherm parameters				Ions measured
				T [K]	*t* [h]	*T* range [K]	*T* step [K]	Equilibration time [min]	Ramp	
α-Ga_2O_3 (s)	2019	41.4	39.2	1622	12	1510–1750	10	5	up/down	Ga^+, Ga^{2+}, Ga^{3+}; GaO^+, Ga_2^+, Ga_2O^+, O_2^+
α-In_2O_3 (s)	2019	42.6	20.3	–	–	1210–1610	10	5	down	In^+, In^{2+}, In^{3+}, InO^+, In_2^+, In_2O^+, O_2^+
α-Ga_2O_3 (s)	2021	46.7	n.d.	–	–	1540–1644 (run 1); 1520–1662 (run 2)	10	5	up (run 1); up/down (run 2)	Ga^+, GaO^+, Ga_2^+, Ga_2O^+, O_2^+
α-In_2O_3 (s)	2021	61.0	n.d.	1295	15	1291–1429 (run 1); 1280–1422 (run 2); 1209–1424 (run 3)	10	5	up/down	In^+, InO^+, In_2^+, In_2O^+, O_2^+

kinetic diameter of 4×10^{-10} m, the effusive limit is reached close to 1 Pa.

The fundamental assumption made in calculating vapour pressures is that the measured partial pressure of any given species p_m remains proportional to that inside the cell p_{eq} in equilibrium with the sample. The degree to which the assumption holds is calculated by the Whitman-Motzfeld equation (eq. (3)):

$$\frac{p_{eq}}{p_m} = 1 + \frac{W_C A}{D}\left(\frac{1}{\alpha_v} + \frac{1}{W_D} - 2\right) \tag{3}$$

where W_C is the Clausing factor of the orifice, A the surface area of the orifice, D that of the cell body, α_v the dimensionless evaporation coefficient and W_D the Clausing factor of the cell body [20,21]. The Clausing factor of the orifice is a scaling factor that accounts for any deviation of the transmission of molecules from the perfect case of an infinitely thin orifice, which is perturbed in a manner following the cosine law ([22]; and references therein). Monte-Carlo simulations have enabled the definition of an empirical relationship between W_C and the thickness/-radius ratio of the orifice, in our case 1, leading to $W_C = 0.67$. Applying the evaporation coefficient $\alpha_v = 0.3 \pm 0.05$ for the evaporation from solid oxides for all gaseous species given in Burns [23], which was determined at the oxides' respective melting points by way of a combination of thermal-imaging and mass-spectrometric techniques for both Ga_2O_3 and In_2O_3, and $W_D = 0.55$, the p_{eq}/p_m in our setup is ~1.006, satisfying the condition that the measured vapour pressure is equivalent to that internal to the cell.

3.1. Determination of partial pressures

Based on the ion intensities obtained from the measurements with KEMS, partial pressures of the species under consideration can be calculated according to eq. (4):

$$p_i = \frac{k I_i T f_i}{\eta_i \gamma_i \sigma_i} \tag{4}$$

Here, p_i describes the partial pressure of species i, k indicates the pressure calibration factor or the instrument sensitivity factor, I_i is the measured intensity of the respective ion, T denotes the temperature in the KC, f_i is the correction factor for fragmentation for Ga or In based on the ratio of M^+ to ΣM^+ with values between 0 and 1, η_i stands for the isotopic abundance of species i, γ_i refers to the multiplier factor of species i and σ_i represents the ionisation cross section of species i. The intensity I_i corresponds to the abundance of a particular ion, *i.e.* M^+, MO^+ or M_2O^+, in the molecular beam that effuses from the Knudsen cell. The value given by the ion counter is directly inserted into eq. (4). Based on the fitting process of the signals obtained, the error of the intensity ΔI_i, is set to 0.25% of the measured value. The isotopic abundance η_i is calculated as the isotopic abundance of the measured mass relative to the total and amounts to 0.60 for ^{69}Ga, to 0.96 for ^{115}In and to 0.99 for ^{16}O (*cf.* Table 2). Where there are several isotopologues (*e.g.* $^{69}Ga^{69}Ga$, $^{69}Ga^{71}Ga$, $^{71}Ga^{71}Ga$), the most abundant was measured. The error of the isotopic abundances $\Delta\eta_i$ is negligible for our purposes.

The instrument sensitivity factor, k, describes the transmission of ions through the mass spectrometer and allows absolute partial pressures to be determined when normalised to the measured intensity of a standard material with known partial pressure at a given temperature. As such, the k value is unique to a given instrument and analytical session, varying over time and with T due to variability in the vacuum conditions, and build-up of deposited material on the apertures [22]. Here, before and after the sample measurements, the accuracy of the pyrometer and instrumental sensitivity factor were determined *in-situ* by means of the determination of *i)* the melting points, T_m, of pure Ag (1235 K) and Ni (1728 K) metal and *ii)* the measured counts (I) of Ag^+ and Ni^+ at T_m.

Temperatures measured by optical pyrometry are plotted against the k values, so that $k(T)$ could be estimated for all investigated temperatures (eq. (5)). The number in parenthesis gives the uncertainty in the last digit.

Measurements Oct. 2019:

$$k = 1.52(6)\times10^{-7}\times T_{pyr} + 2.9(6)\times10^{-5} \tag{5a}$$

Measurements Nov. 2021:

$$k = 1.89(3)\times10^{-7}\times T_{pyr} - 6.6(3)\times10^{-5} \tag{5b}$$

The error in the pyrometer temperature reading is ±5 K. The uncertainty of k reflects the fact that measurements were performed over a long time interval for the first measurements runs from October 2019 and February 2020, and that only two points were used to determine the change in k with temperature.

Measured melting points for Ag and Ni are plotted *vs.* the melting points given in literature and the equation (eq. (6)) obtained from linear regression is applied for the estimation of the real temperature T_{real}.

$$T_{real} = 1.060(4)\times T_{pyr} + 53(4) \tag{6}$$

This procedure was applied only for the measurements made in October 2019, whereas the temperature measurements from November 2021, using a different KEMS device, were within uncertainty of the literature values.

The multiplier factor γ_i describing a mass- and molecule structure-dependent value of secondary electron emission from the first dynode of a multiplier is set to a value of 1 for both elements, since an ion counting system was applied in the KEMS. The error of the multiplier factor γ_i, $\Delta\gamma_i$, is assumed to be 0. Ionisation by electron impact occurs by ejection of one or more electrons from the species, resulting in singly (eq. (7)) or multiply charged ions (eqs. (8) and (9)) with the ionisation energy required in each step increasing progressively from reaction (7) to (9).

$$M\,(g) + e^- = M^+(g) + 2e^- \tag{7}$$

$$M^+(g) + e^- = M^{2+}(g) + 2e^- \tag{8}$$

$$M^{2+}(g) + e^- = M^{3+}(g) + 2e^- \tag{9}$$

The ionisation cross section, σ_i of the parent species is a measure of the probability that the parent molecule of that species is ionised by electron impact at a given ionisation energy. This quantity has been determined by means of different models (*cf.* [24–26]) as well as experimentally [27]. Since the resulting estimates for σ_i exhibit a large spread, an average over all methods was taken to weight the mean ionisation cross section (*cf.* Tables 4 and 5) and its standard deviation was included in the error calculation for the partial pressures. Given that the difference in cross sections at the energies measured (60 eV and 70 eV) is negligible and within the standard deviation, *e.g.* 7.48 at 60 eV and 7.03 at 70 eV in Jacobson [25] and in Deutsch et al. [26] at a standard deviation of ±1.38 (Table 4), and hence within the standard deviation, the cross sections obtained at 60 eV are applied for all measurements.

For molecular oxygen, not listed in Table 4 or 5, a cross section of $\sigma(O_2) = 2.8$ is used [32]. As no error is given, an error of 17% (= 0.5) is assumed, based on errors of other cross sections. Occasionally, ionisation leads to fragmentation, which describes the break-up of a complex molecule into simpler constituents [15,33]. Such fragmentation may be detected by the measurement of ionisation efficiency curves, which are constructed by scanning the electron energy from 0 to 70 eV at constant T and measuring the ion intensity. Ionisation efficiency curves of the different species measured herein exhibit clear indications of fragmentation via electron-impact (*cf.* Fig. 2). Accordingly, the signal measured for a particular ion (*e.g.* M^+) may also contain contributions derived not only from the equilibrium atom, M^0, but also from different polyatomic molecules, such as M_2O^0, by a reaction of the type (eq. (10)):

Table 4
Summary of ionisation cross sections for different Ga species at 60 eV.

Reference	σ (Ga^+) [Å^2]	σ (GaO^+) [a, b] [Å^2]		σ (Ga_2^+) [a, c] [Å^2]		σ (Ga_2O^+) [a, d] [Å^2]	
Freund et al. [27]	8.62	7.67	5.75	12.93	12.93	14.13	14.37
Jacobson [25]; Deutsch et al. [26]	7.48	6.81	4.99	11.22	11.22	12.42	12.46
Bonnell and Hastie [24]	5.73	5.50	3.82	8.59	8.59	9.79	9.54
Kim and Stone [28]	9.47	8.30	6.31	14.21	14.21	15.41	15.79
Margreiter et al. [29]	7.39	6.74	4.93	11.08	11.08	12.28	12.31
Patton et al. [30]	9.07	8.00	6.05	13.61	13.61	14.81	15.12
Mean	**7.96**	**6.24**		**11.94**		**13.20**	
Standard deviation	1.38	1.35		1.97		2.08	

[a] Left column: Jacobson [25], sum of atomic cross sections multiplied by a correction factor of 0.75; σ(O) = 1.6 Å^2 according to Drowart and Goldfinger [15].

[b] Right column: Gomez et al. [9], assumption that $\sigma\left(\frac{M}{MO}\right) = 1.5$

[c] Right column: Drowart and Goldfinger [15], assumption that $\sigma\left(\frac{M_2}{M}\right) = 1.5$

[d] Right column: Gomez et al. [9], assumption that $\sigma\left(\frac{MO}{M_2O}\right) = 0.4$

Table 5
Summary of ionisation cross sections for different In species at 60 eV.

Reference	σ (In^+) [Å^2]	σ (InO^+) [a, b] [Å^2]		σ (In_2^+) [a, c] [Å^2]		σ (In_2O^+) [a, d] [Å^2]	
Freund et al. [27]	10.44	9.03	6.96	15.66	15.66	16.86	17.4
Jacobson [25]; Deutsch et al. [26]	9.62	8.41	6.41	14.42	14.42	15.62	16.03
Bonnell and Hastie [24]	7.53	6.85	5.02	11.30	11.30	12.50	12.55
Kim and Stone [28]	11.57	9.88	7.71	17.35	17.35	18.55	19.28
Margreiter et al. [29],	9.56	8.37	6.37	14.33	14.33	15.53	15.93
Lotz [31][e]	5.64	5.43	3.76	8.46	8.46	9.66	9.40
Mean	**9.74**	**7.50**		**14.61**		**16.03**	
Standard deviation	1.48	1.45		2.09		2.22	

[a] Left column: Jacobson [25], sum of atomic cross sections multiplied by a correction factor of 0.75; σ(O) = 1.6 Å^2 according to [15].

[b] Right column: Gomez et al. [9], assumption that $\sigma\left(\frac{M}{MO}\right) = 1.5$

[c] Right column: Drowart and Goldfinger [15], assumption that $\sigma\left(\frac{M_2}{M}\right) = 1.5$

[d] Right column: Gomez et al. [9], assumption that $\sigma\left(\frac{MO}{M_2O}\right) = 0.4$

[e] Excluded for the calculation of the average and the standard deviation.

$$M_2O + e^- = M^+ + MO + 2e^- \quad (10)$$

Gomez et al. [9] showed that the above reaction is energetically more favourable for In species than for the fragmentation of $In_2O + e^-$ into $InO^+ + In + 2e^-$. Hence, a correction factor f_i is introduced to derive partial pressures from ion intensities. In order to quantify the degree of fragmentation, we compare the appearance potentials of the ions of potential parent molecules (Ga_2O^+ and In_2O^+) with the observed ionisation efficiency curve for their respective daughter ions (Ga^+ and In^+) (Fig. 2).

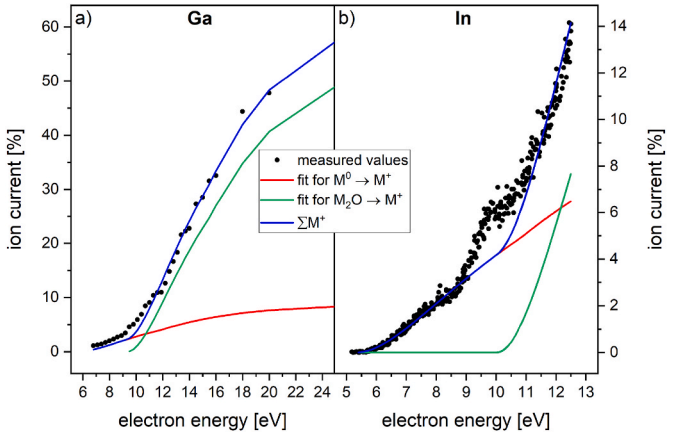

Fig. 2. Ionisation efficiency curves measured for a) Ga^+ and b) In^+ above pure Ga_2O_3 and pure In_2O_3, respectively, with fits calculated according to the expressions given by Jacobson [25].

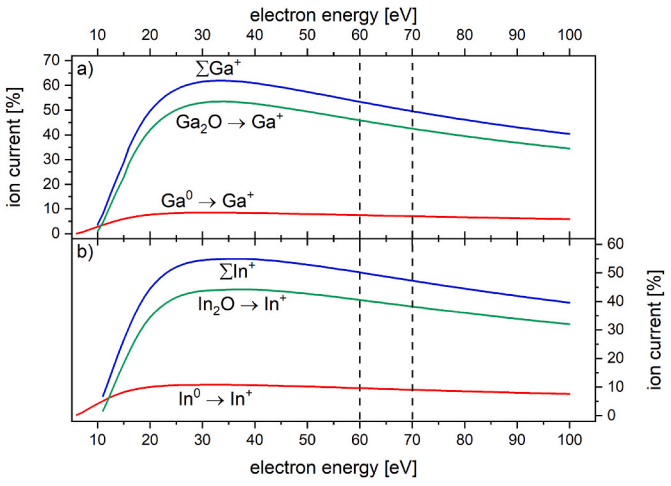

Fig. 3. Ionisation efficiency curves for M^0 and M_2O^0, fitted and extrapolated according to Jacobson [25]. Dashed black lines mark electron energy used within the experiments.

The resulting ion intensities as a function of electron energy can be assigned to different ionisation processes by simultaneously monitoring the signals of M^+ and M_2O^+. The data up to ~12 eV for Ga (Fig. 2a) and up to ~9 eV for In (Fig. 2b), represent M^+ ions that originate from M atoms (red line), whereas above 12 or 9 eV, respectively, the M^+ signal comprises the sum of M^+ (blue line) that results from fragmentation of M_2O molecules (green line) and M. These assignments are made because the appearance potentials of M_2O^+ (which can only result from the ionisation of M_2O) are higher by ~4.5 eV ($dE_{green\text{-}blue} = E_{green} - E_{blue}$) than those of the corresponding M^+, as determined by monitoring M_2O^+. "The imperfection in the supposedly linear section" of the ion efficiency curve of In at ~10 eV (Fig. 2b) is not the result of a further ionisation process, but an instrumental issue that was recognised in the measurements of Gomez et al. [9]. They suggest additional electric tuning of the ionisation source to avoid such imperfections. The data are fit with the ionisation cross section equations of Jacobson [25], based on a least-squares method in which the contributions of M and M_2O-derived signals are varied to minimise the misfit to the observations (Fig. 3).

Calculating the ratio of the M^+ intensities resulting from M^0 and M_2O^0 (red and blue curves, Figs. 2 and 3) at 60 eV (measurements in October 2019) or 70 eV (measurements in November 2021), leads to a correction factor f_i of 0.14 for Ga^+ and of 0.19 for In^+. The intensity measured for M^+ is subsequently multiplied with the correction factor f_i to exclude the apparent contribution from the fragmentation of M_2O^0. The resulting intensity of M^+, reflecting that solely from ionisation of M^0, is multiplied by the ionisation cross section of M^+ according to eq. (4) to obtain p(M). No correction is needed for MO^+, *i.e.* f_i is equal to 1. Regarding M_2^+, we deduce that all the signal stems from the fragmentation of M_2O^+, leading to f_i for M_2^+ of 0. In the case of M_2O^+, the correction is (eq. (11)),

$$p_{M_2O,\ corr.} = p_{M_2O,\ orig.} + \left(p_{M,\ orig.} \times (1 - f_{M^+})\right) + \left(p_{M_2,\ orig.} \times \left(1 - f_{M_2^+}\right)\right) \tag{11}$$

where $p_{M_2O,\ corr.}$ is the corrected partial pressure, original in $p_{M_2O,\ orig.}$ refers to the initial partial pressure calculated from the specific ion intensity assuming $f_i = 1$, while f_{M^+} is either 0.14 for Ga or 0.19 for In, respectively and $f_{M_2^+}$ is 0. The partial pressure $p_{M_2O,\ orig.}$ is calculated using the cross section of M_2O^+, the partial pressure $p_{M,\ orig.}$, which is only used in this context and is not the same as p(M), is calculated using the cross section of M^+, even though it also contains a contribution from fragmentation of M_2O^0. The error of the correction factor f_i, Δf_i, amounts to 0.1 for all species, based on the accuracy and precision of the ionisation efficiency curves. The partial pressure of oxygen is not obtained by means of a measured intensity, but determined by stoichiometry according to the measured p(M), p(MO), $p(M_2)$ and $p(M_2O)$. The calculation is based on the Hertz-Knudsen equation (eq. (12), [34,35]), and illustrated here using the example of p(Ga) [14].

$$\frac{dn_i}{dt} = \frac{p_i A_0}{\sqrt{2\pi M_i RT}} \tag{12}$$

Here, n_i denotes the moles of species i, t the time, A_0 the area of the hole in the lid of the Knudsen cell, M_i the molar mass of the evaporating species i, R the molar gas constant and T is temperature in K. Due to the fact that the rate of effusion is constant $\left(\frac{dn_i}{dt} = c\right)$ at a given temperature and for a given species, eq. (12) can be simplified to eq. (13) [14].

$$p_i \sim \sqrt{M_i} \tag{13}$$

Considering the stoichiometric coefficients resulting from the respective evaporation reactions, the following relation can be established (eq. (14), [14]).

$$\frac{p(\mathrm{Ga})}{p_{\mathrm{Ga}}(\mathrm{O_2})} = \frac{4}{3}\frac{\sqrt{M(\mathrm{Ga})}}{\sqrt{M(\mathrm{O_2})}} \tag{14}$$

The partial pressure of O_2 derived from that of Ga, $p_{Ga}(O_2)$, is thus given by (eq. (15)):

$$p_{\mathrm{Ga}}(\mathrm{O_2}) = \frac{3}{4}\frac{\sqrt{M(\mathrm{O_2})}}{\sqrt{M(\mathrm{Ga})}}p(\mathrm{Ga}) = 0.51\ p(\mathrm{Ga}) \tag{15}$$

Oxygen partial pressures may be derived from all other species analogously, the respective equations are summarised in Table 6.

The total partial pressure of oxygen $p(O_2)$ is subsequently obtained as sum of the partial pressures of oxygen produced from the evaporation of the different M-bearing species (eq. (16)).

$$p(\mathrm{O_2}) = p_{\mathrm{M}}(\mathrm{O_2}) + p_{\mathrm{MO}}(\mathrm{O_2}) + p_{\mathrm{M_2}}(\mathrm{O_2}) + p_{\mathrm{M_2O}}(\mathrm{O_2}) \tag{16}$$

The total error for the partial pressure of a particular species is calculated according to eq. (17).

$$\Delta p_i = \left|\frac{I_i T f}{\eta_i \gamma_i \sigma_i}\Delta k\right| + \left|\frac{kTf}{\eta_i \gamma_i \sigma_i}\Delta I_i\right| + \left|\frac{kI_i f}{\eta_i \gamma_i \sigma_i}\Delta T\right| + \left|\frac{kI_i T}{\eta_i \gamma_i \sigma_i}\Delta f\right| + \left| - \frac{kI_i Tf}{\eta_i^2 \gamma_i \sigma_i}\Delta \eta_i\right| + \left| - \frac{kI_i Tf}{\eta_i \gamma_i^2 \sigma_i}\Delta \gamma_i\right| + \left| - \frac{kI_i Tf}{\eta_i \gamma_i \sigma_i^2}\Delta \sigma_i\right| \tag{17}$$

3.2. Determination of equilibrium constants, changes of enthalpies and entropies of reaction and enthalpies of formation

The partial pressures are used to calculate equilibrium constants K for the decomposition reactions of M_2O_3(s) into the individual M-bearing species and O_2. An example is shown for the congruent dissociative evaporation of M_2O_3(s) to 2 M(g) and 1.5 O_2(g) in eq. (18) and eq. (19), where p^0 is the standard state pressure of 10^5 Pa and the activity a of M_2O_3 is equal to 1.

$$\mathrm{M_2O_3(s) = 2\ M(g) + 1.5\ O_2(g)} \tag{18}$$

$$K = \frac{\left(\frac{p(\mathrm{M})}{p^0}\right)^2 \left(\frac{p(\mathrm{O_2})}{p^0}\right)^{1.5}}{a(\mathrm{M_2O_3})} \tag{19}$$

Owing to the fact that the change of Gibbs free energy of reaction, $\Delta_r G$, is 0 at equilibrium, the following equation (eq. (20)) holds:

$$\Delta_r G_T^{\circ} = -RT\ln(K) = \Delta_r H_T^{\circ} - T\Delta_r S_T^{\circ} \tag{20}$$

with $\Delta_r G_T^{\circ}$ being the change of Gibbs free energy of reaction at the standard pressure p^0 and the mean T of the measurement. By rearranging eq. (20), equilibrium constants can be used to determine $\Delta_r H_T^{\circ}$ and $\Delta_r S_T^{\circ}$ as the slope and intercept, respectively, in a van't Hoff plot (eqs. (21)–(23)). This is referred to as the '2nd-law method' [36].

$$\ln(K) = -\frac{\Delta_r H_T^{\circ}}{R}\frac{1}{T} + \frac{\Delta_r S_T^{\circ}}{R} \tag{21}$$

$$\Delta_r H_{T,\ 2nd}^{\circ} = -slope \times R \tag{22}$$

$$\Delta_r S_{T,\ 2nd}^{\circ} = intercept \times R \tag{23}$$

Since the results for $\Delta_r H_{T,\ 2nd}^{\circ}$ are valid at the average T of the measurement, a comparison of different measurements is only possible to a

Table 6
Summary of equations for the calculation of $p(O_2)$.

$p(O_2)$ derived from species	Equation
$p_{Ga}(O_2)$	0.51 p(Ga)
$p_{GaO}(O_2)$	0.15 p(GaO)
$p_{Ga_2}(O_2)$	0.72 $p(Ga_2)$
$p_{Ga_2O}(O_2)$	0.45 $p(Ga_2O)$
$p_{In}(O_2)$	0.40 p(In)
$p_{InO}(O_2)$	0.12 p(InO)
$p_{In_2}(O_2)$	0.56 $p(In_2)$
$p_{In_2O}(O_2)$	0.36 $p(In_2O)$

certain extent. Therefore, the van't Hoff equation (eq. (24)) is integrated from $T = 0$ K to $T = 298$ K (eq. (25)).

$$\frac{d \ln K(T)}{dT} = \frac{\Delta_r H^{\circ}_{T,\ 2nd}}{RT^2} \tag{24}$$

$$\int_{\ln K(0K)}^{\ln K(298\ K)} d \ln K(T) = \frac{\Delta_r H^{\circ}_{T,\ 2nd}}{R} \int_{0\ K}^{298\ K} \frac{1}{T^2} dT \tag{25}$$

Since eq. (26) applies at $T \rightarrow 0$ K, with $\Delta_r G^{\circ}(0)$ as Gibbs free energy at 0 K:

$$-RT \ln(K(T)) = \Delta_r G^{\circ}(0) = \Delta_r H^{\circ}(0) \tag{26}$$

Then, using Gibbs energy functions referenced to 298 K, $gef^{\circ}_{298}(T)$, at T of the measurement (eq. (27)), where $H^{\circ}(T)$ and $S^{\circ}(T)$ are the enthalpy and entropy at the standard-state pressure of 1 bar and temperature T and H°_{298} is the reference enthalpy at the standard-state pressure and temperature (1 bar and 298 K), one obtains

$$gef^{\circ}_{298}(T) = -S^{\circ}(T) + \frac{H^{\circ}(T) - H^{\circ}_{298}}{T} \tag{27}$$

At equilibrium for a reaction, Gibbs energy functions of reaction referenced to 298 K, $\Delta_r gef^{\circ}_{298}(T)$, at T of the measurement, are calculated based on the Gibbs energy functions for the individual species according to the stoichiometry of the reactions investigated (eq. (28)):

$$\Delta_r gef^{\circ}_{298}(T) = \sum gef^{\circ}_{298}(T, products) - \sum gef^{\circ}_{298}(T, reactants) \tag{28}$$

One then obtains the following relation (eq. (29); *cf.* [36]; for more details):

$$-R \ln(K(T)) - \Delta_r gef^{\circ}_{298}(T) = \Delta_r H^{\circ}_{298,\ 2nd} \frac{1}{T} + \Delta_r S^{\circ}(0) \tag{29}$$

$\Delta_r H^{\circ}_{298,\ 2nd}$ is obtained as the slope in a plot of $-R \ln(K(T)) - \Delta_r gef^{\circ}_{298}(T)$ *vs.* $\frac{1}{T}$ and can be compared between all measurements [36]. The value of the intercept, $\Delta_r S^{\circ}(0)$, is a measure of the consistency of the 2nd- and the 3rd-law results, as it is straightforward to show that when $\Delta_r S^{\circ}(0) = 0$, then $\Delta_r H^{\circ}_{298,\ 2nd}$ approaches the one obtained via the '3rd-law method' (eq. (30)).

$$\Delta_r H^{\circ}_{298,\ 3rd} = -RT \ln(K(T)) - T\Delta_r gef^{\circ}_{298}(T) \tag{30}$$

The advantage of the '3rd-law method' is that the enthalpy of reaction can be calculated from a single measurement [36] and does not assume constant $\Delta_r H^{\circ}_T$ over the temperature interval of the measurements.

Enthalpies of formation $\Delta_f H^{\circ}_{298}(i)$ are calculated from $\Delta_r H^{\circ}_{298}$ by rearranging eq. (31).

$$\Delta_r H^{\circ}_{298} = \sum \Delta_f H^{\circ}_{298}(products) - \sum \Delta_f H^{\circ}_{298}(reactants) \tag{31}$$

4. Results

4.1. X-ray diffraction

According to XRD analysis (*cf.* section 2.2.2 and diffractograms in the Appendix), our starting material consisted mainly of α-Ga_2O_3 (Fig. 12), but transformed into β-Ga_2O_3 (Fig. 13) following heating ($T_{max.} = 1480$ °C), as only β-Ga_2O_3 is stable above 870 °C. In contrast, no transformation was observed for In_2O_3 (Figs. 14 and 15), which remained as α-In_2O_3 as the experiments were conducted at 10^{-6} mbar. For a transformation into β-In_2O_3 a pressure of 3.8 GPa would have been needed [7]. These results are in partial disagreement with those reported by Shchukarev et al. [8], who state that "The X-ray diffraction patterns of the initial oxides and the oxides heat-treated in a vacuum were completely identical and did not exhibit any lines other than those of the M_2O_3 lattices, (…)". In addition, the XRD analyses provided no evidence for any interaction between Ga_2O_3 or In_2O_3 with the Ir cell material.

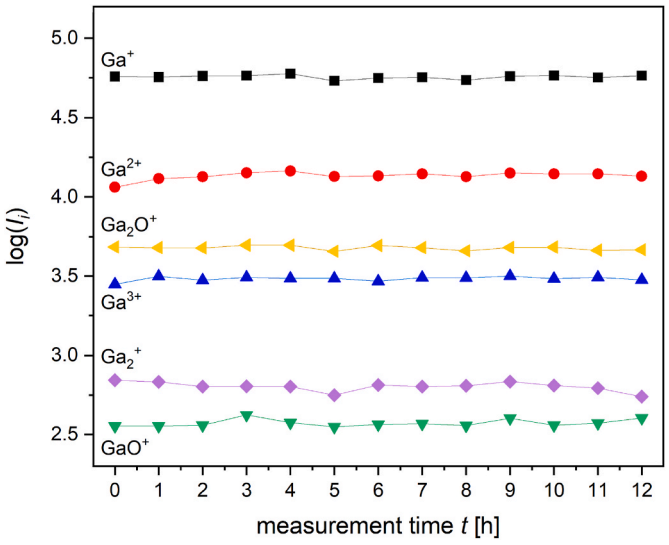

Fig. 4. Isotherm measurement showing the intensities of different Ga-bearing ions at 1622 K for 12 h.

Table 7
Average intensities and standard deviations of the isotherm measurement.

Ion	Average intensity [cps]	Standard deviation [cps]
Ga^+	57061	1569
Ga^{2+}	13615	749
Ga^{3+}	3042	98
GaO^+	374	21
Ga_2^+	638	43
Ga_2O^+	4782	146

4.2. KEMS - Isotherm

In order to assess whether the sensitivity of the instrument and/or the relative abundances of vapour species changed over the course of the measurements, and thus to determine the timescale for the system (condensed phase plus vapour) to reach thermal equilibrium inside the KC, an isotherm measurement was performed for 12 h at 1622 K with Ga_2O_3 (s) (Fig. 4).

The intensities of the Ga-bearing species under consideration are stable, at least over the entire measurement of 12 h within the standard deviation given in Table 7.

4.3. KEMS - Polytherm

4.3.1. Partial pressures

Partial pressures of three different Ga-bearing species (Ga, GaO and Ga_2O) are calculated with eq. (4) from the intensities measured above heated Ga_2O_3 within a temperature range of 1510–1752 K, as displayed in Fig. 5.

Among Ga-bearing species, Ga_2O exhibits by far the highest partial pressures (0.79 ± 0.3 Pa at 1752 K), followed by Ga, whose partial pressure is lower by a factor of 7 (0.11 ± 0.016 Pa at 1752 K). The partial pressures of GaO (0.007 ± 0.002 Pa) are several orders of magnitude lower again at the same temperature. The partial pressure of Ga_2O is roughly an order of magnitude lower than that reported by Shchukarev et al. [8] at similar temperatures (their Table 2). The $\ln(p_i)$ of Ga-bearing species increase roughly linearly with reciprocal temperature. The different runs yield concordant values for p(Ga), p(GaO) and p(Ga_2O)

Table 8
Summary of the thermodynamic quantities calculated from the measurements carried out within the framework of this study as well as from partial pressures given in literature for reactions involving Ga-bearing species.

T_{mean} [K]	$\Delta_r H^{\circ}_{T,\ 2nd}$ [Jmol^{-1}]	$\Delta_r S^{\circ}_{T,\ 2nd}$ [Jmol^{-1}K^{-1}]	$\Delta_r H^{\circ}_{298,\ 2nd}$ [Jmol^{-1}]	$\Delta_r H^{\circ}_{298,\ 3rd}$ [Jmol^{-1}]	Ref.
$\mathbf{Ga_2O_3(s) = 2\ Ga(g) + 1.5\ O_2(g)}$					
1633 ± 14	1839061 ± 34238	667 ± 21	1879251 ± 35410	1656486 ± 25272	Oct19
1592 ± 12	1587946 ± 70722	516 ± 45	1626920 ± 71167	1651766 ± 21895	Nov21#1
1596 ± 12	1714571 ± 52776	594 ± 33	1753483 ± 53384	1653861 ± 21951	Nov21#2
			1753218 ± 126122	1654037 ± 2365	*Mean*
1623	1603016	529	1642674	1646749	Hult73
$\mathbf{Ga_2O_3(s) = 2\ GaO(g) + 0.5\ O_2(g)}$					
1633 ± 14	1359042 ± 39837	451 ± 25	1387484 ± 40597	1386648 ± 23010	Oct19
1593 ± 12	1147903 ± 62997	319 ± 40	1175728 ± 63291	1384782 ± 19924	Nov21#1
1603 ± 12	1368728 ± 61914	455 ± 39	1396546 ± 62312	1388754 ± 19978	Nov21#2
			1319920 ± 124955	1386728 ± 1987	*Mean*
1623	1349511	436	1377643	1400743	Medv81
$\mathbf{Ga_2O_3(s) = Ga_2O(g) + O_2(g)}$					
1633 ± 14	1056395 ± 23228	402 ± 14	1105858 ± 24064	1028532 ± 18878	Oct19
1592 ± 12	879954 ± 42121	301 ± 27	928034 ± 42543	1014368 ± 15903	Nov21#1
1596 ± 12	958837 ± 34354	349 ± 22	1006847 ± 34832	1017487 ± 16009	Nov21#2
			1013580 ± 89103	1020129 ± 7442	*Mean*
1623	946935	352	995780	1000099	Chap75
1790	1036962	425	1092211	961018	Shch69

References.
Chap75: p_i from FACTSAGE database, based on Chaplygin [37] and Medvedev et al. [38].
Hult73: p_i from FACTSAGE database, based on Hultgren et al. [39].
Mean: Mean of the measurements carried out within this work.
Medv81: p_i from FACTSAGE database, based on Medvedev et al. [38].
Nov21#1–2: This work, measurement from November 2021, run 1-2.
Oct19: This work, measurement from October 2019.
Shch69: p_i from Shchukarev et al. [8].

within error.

The partial pressures of In-bearing species above heated In_2O_3 were investigated between 1210 K and 1611 K (Fig. 6). The sequence of the partial pressures of In-bearing species mirrors that for Ga-bearing gases, from In_2O (1.41 ± 0.52 Pa at 1611 K), then In (0.30 ± 0.05 Pa) to InO (0.0036 ± 0.001 Pa). This order is in qualitative agreement with the literature results of Gomez et al. [9] and Smirnov et al., [10], who also find In_2O to be the most abundant gas species above solid In_2O_3. Quantitatively, the partial pressures are in agreement with Smirnov et al. [10], *i.e.* $p(In_2O) = 1.3$ Pa and $p(In) = 0.46$ Pa at 1600 K, but these are a factor of ~3 lower than those determined by Gomez et al. [9] at the same temperature. As per Ga, $\ln(p_i)$ rises approximately linearly with reciprocal temperature for all species and the agreement between the individual measurement runs made in Oct. 2019 and Nov. 2021 is excellent for p(In) and p(InO), but slightly outside error for $p(In_2O)$ only at the lowest temperatures. Comparing the vaporisation behaviour of the two oxides Ga_2O_3 and In_2O_3, p_i of the dominant species in the vapour phase (Ga_2O and In_2O) reaches ~1 Pa (the effusion limit) at 150 K lower T for In_2O_3 compared to Ga_2O_3.

4.3.2. Equilibrium constants

Single partial pressures p_i do not allow a robust comparison to be made between different measurements, owing to the fact that they depend on the partial pressure of oxygen $p(O_2)$. For this reason, we compare equilibrium constants K of vaporisation reactions (*cf.* eq. (19)) with those reported in literature in a $\ln(K)$ *vs.* $1/T$ space (Fig. 7, Ga-bearing species; Fig. 8, In-bearing species).

Equilibrium constants obtained from the measurements for the evaporation reaction of $Ga_2O_3(s) = 2\ Ga(g) + 1.5\ O_2(g)$, abbreviated as $K_{meas.}$(Ga), are in excellent agreement with the data compiled in FACTSAGE $K_{lit.}$(Ga) [39]. More precisely, the values are within uncertainty above 1650 K, at lower T $K_{lit.}$(Ga) slightly exceeds $K_{meas.}$(Ga) (Fig. 7b). The values of $K_{meas.}$(GaO) exhibit some scatter below 1550 K owing to the very low ion intensities of GaO^+ at low temperatures, and in general exhibit higher values than $K_{lit.}$(GaO) from FACTSAGE [38] (Fig. 7c). For Ga_2O, K based on the measurements are lower than those from literature [37,38], the difference decreasing towards higher T (Fig. 7a). Estimates of $K(Ga_2O)$ from the partial pressures given in Shchukarev et al. [8] are about an order of magnitude higher than $K_{meas.}(Ga_2O)$, and a factor of 4 higher than $K_{lit.}(Ga_2O)$ from FACTSAGE. The robustness and quality of the data in FACTSAGE (*cf.* section 5.5) is difficult to assess, as no details on their determination are available.

For the In-bearing species (Fig. 8), the differences to FACTSAGE are larger than for Ga-bearing species. The values of $K_{meas.}$ are lower than $K_{lit.}$ from FACTSAGE for all species over the entire T range investigated. Significant discrepancies among literature studies are observed, too, also for different runs reported from the same study, *e.g.* for $K_{lit.}$(In) (Fig. 8b). The different measurement runs reported in this work are within error of one another. Moreover, our data match those reported in the most recent determination of equilibrium constants of In_2O_3(s) vaporisation reactions measured by KEMS [10]. As observed for GaO, $K_{meas.}$(InO) (Fig. 8 c)) scatters at low temperatures (up to 1350 K), and our $K_{meas.}$(InO) is lower than $K_{lit.}$(InO) from Gomez et al. [9], which are in turn lower than $K_{lit.}$(InO) from FACTSAGE [40]. On the other hand, $d(\ln(K_{meas.}(InO)))/d(1/T)$ and $d(\ln(K_{lit.}(InO)))/d(1/T)$ from FACTSAGE are sub-equal, whilst the values from Gomez et al. [9] are a little flatter. Concerning In_2O (Fig. 8 a), our equilibrium constants are slightly lower than those reported by Burns [23], Shchukarev et al. [8], Gomez et al. [9] and FACTSAGE [37,38], as for Ga_2O. However, they are in excellent agreement with the results of Smirnov et al. [10].

4.3.3. Enthalpy and entropy of reaction

Van't Hoff plots of the equilibrium constants K *vs.* reciprocal T (Figs. 7 and 8) enable the determination of $\Delta_r H^{\circ}_{T,\ 2nd}$ and $\Delta_r S^{\circ}_{T,\ 2nd}$ by linear regression (eq. (21), 2nd-law method), plotting $-R\ln(K(T)) - \Delta_r gef^{\circ}(T)$ *vs.* reciprocal T leads to $\Delta_r H^{\circ}_{298,\ 2nd}$ (eq. (29)). Results are listed in Tables 8 and 9. Values of $\Delta_r H^{\circ}_{298,\ 3rd}$ from the 3rd-law method (eq. (30)) are calculated based on $\Delta_r gef^{\circ}_{298}(T)$ estimated from FACTSAGE database (eqs. (27) and (28)). Results are plotted in Figs. 9 and 10 and summarised in Tables 8 and 9. In order to facilitate comparison with this work, we recalculate the values of $\Delta_r H^{\circ}_{298,\ 3rd}$ from the raw p_i reported in Gomez et al. [9] and Smirnov et al. [10] by applying $\Delta_r gef^{\circ}_{298}(T)$ from

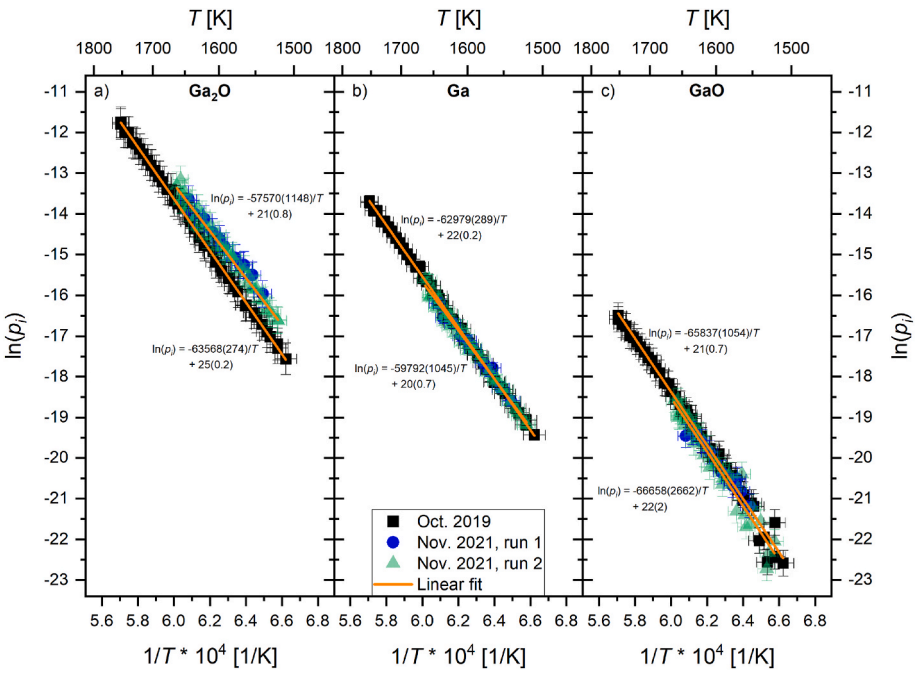

Fig. 5. Partial pressures of Ga-bearing species a) Ga_2O, b) Ga and c) GaO above heated Ga_2O_3, determined within a temperature range of 1510–1752 K.

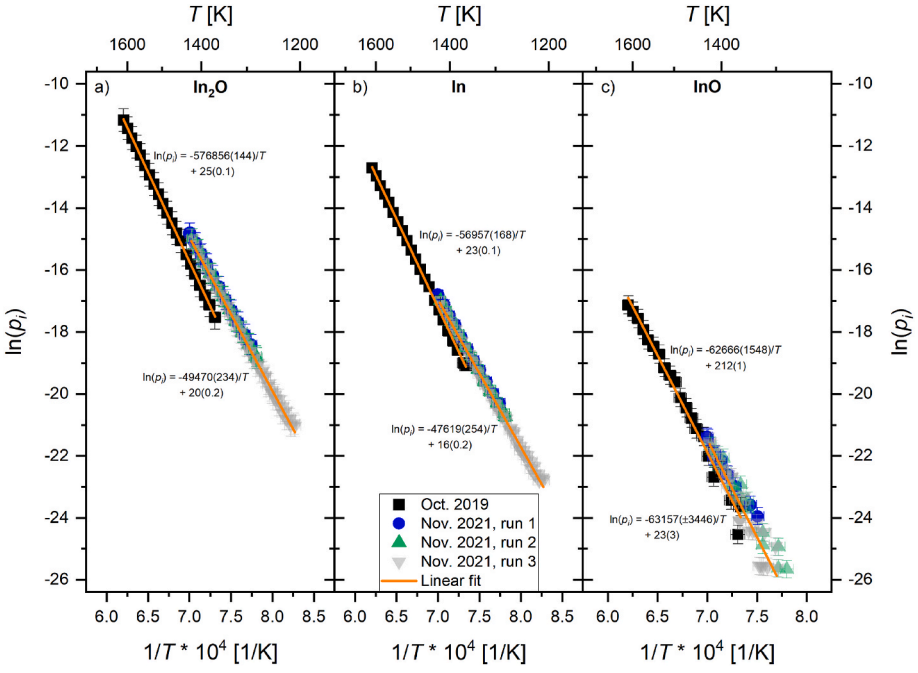

Fig. 6. Partial pressures of In-bearing species a) In_2O, b) In and c) InO above heated In_2O_3, quantified within a temperature range of 1210–1611 K.

FACTSAGE, as we did analogously for our own data. The original results reported in Gomez et al. [9] or Smirnov et al. [10], calculated from raw p_i based on their own method and thermodynamic data, are listed in parentheses in Table 9.

Since $\Delta_r H^{\circ}_{298,\,2nd}$ exhibits a much larger spread in between the results for single measurement runs carried out within this work, which becomes obvious when comparing standard deviations for $\Delta_r H^{\circ}_{298,\,2nd}$ and $\Delta_r H^{\circ}_{298,\,3rd}$ (*e.g.* $\Delta_r H^{\circ}_{298,\,2nd} = 1753218 \pm 126122$ Jmol^{-1} and $\Delta_r H^{\circ}_{298,\,3rd} = 1654037 \pm 2365$ Jmol^{-1} for the reaction $Ga_2O_3(s) = 2\,Ga(g) + 1.5\,O_2\,(g)$) and in general is in worse agreement with literature results (*cf.* $\Delta_r H^{\circ}_{298,\,2nd} = 1753218 \pm 126122$ Jmol^{-1} and $\Delta_r H^{\circ}_{298,\,3rd} = 1654037 \pm 2365$ Jmol^{-1} *vs.* $\Delta_r H^{\circ}_{298,\,2nd} = 1642674$ Jmol^{-1} and $\Delta_r H^{\circ}_{298,\,3rd} = 1646749$ Jmol^{-1} from Hultgren et al. [39] for the reaction $Ga_2O_3(s) = 2\,Ga(g) + 1.5\,O_2\,(g)$), only $\Delta_r H^{\circ}_{298,\,3rd}$ is recommended for further application.

4.3.4. *Enthalpy of formation*

Enthalpies of formation $\Delta_f H^{\circ}_{298}(i)$ are calculated from enthalpies of reaction $\Delta_r H^{\circ}_{298}$ according to eq. (31). Results for Ga-bearing species are given in Table 10. $\Delta_f H^{\circ}_{298}(Ga_2O_3(s)) = -1089095$ Jmol^{-1}, $\Delta_f H^{\circ}_{298}(Ga(g)) = 271960$ Jmol^{-1} and $\Delta_f H^{\circ}_{298}(O(g)) = 249173$ Jmol^{-1} needed for calculations are obtained via the empirical equation given in

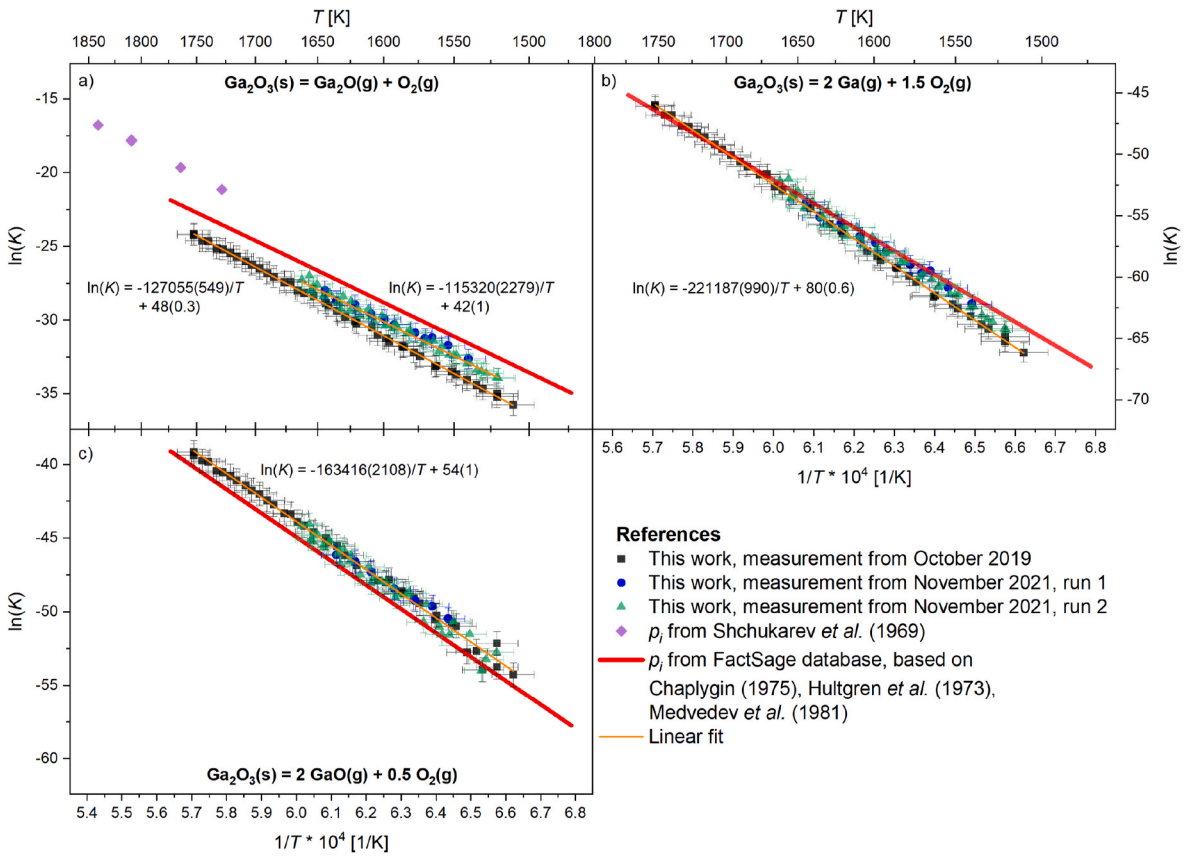

Fig. 7. ln(K) for the reactions of Ga_2O_3 into a) Ga_2O, b) Ga and c) GaO plotted *vs.* reciprocal T for measured and literature data.

the software FACTSAGE, the bonding energy for GaO of 4.06 eV related to the reaction GaO(g) = Ga(g) + O (g) is taken from Petsalakis et al. [41]. The original results reported in Shchukarev et al. [8], calculated from raw p_i based on their own method and thermodynamic data, are listed in parentheses.

$\Delta_f H^{\circ}_{298}(i)$ for In-bearing species is calculated from $\Delta_f H^{\circ}_{298}(In_2O_3(s)) = -925789$ Jmol^{-1}, $\Delta_f H^{\circ}_{298}(In(g)) = 244609$ Jmol^{-1} and $\Delta_f H^{\circ}_{298}(O(g)) = 249173$ Jmol^{-1}, which are also obtained from FACTSAGE, and from a bonding energy for InO of 3.48 eV related to the reaction InO(g) = In(g) + O (g) [42]. Results are summarised in Table 11, numbers in parentheses represent the original values reported in Gomez et al. [9] and Smirnov et al. [10].

As shown in section 4.3.3 for the enthalpy of reaction based on 2nd-law method, $\Delta_r H^{\circ}_{298,\ 2nd}$, the enthalpy of formation based on 2nd-law method, $\Delta_f H^{\circ}_{298,\ 2nd}(i)$, also exhibits a much larger spread in between the results for single measurement runs carried out within this work than $\Delta_f H^{\circ}_{298,\ 3rd}(i)$ from 3rd-law method (*cf.* standard deviations of $\Delta_f H^{\circ}_{298,\ 2nd}(Ga) = 332061 \pm 63083$ Jmol^{-1} and $\Delta_f H^{\circ}_{298,\ 3rd}(Ga) = 282471 \pm 1183$ Jmol^{-1}) as well as generally larger discrepancies from literature data (*cf.* $\Delta_f H^{\circ}_{298,\ 2nd}(Ga) = 332061 \pm 63083$ Jmol^{-1} and $\Delta_f H^{\circ}_{298,\ 3rd}(Ga) = 282471 \pm 1183$ Jmol^{-1} *vs.* $\Delta_f H^{\circ}_{298,\ 2nd}(Ga) = 276789$ Jmol^{-1} and $\Delta_f H^{\circ}_{298,\ 3rd}(Ga) = 278827$ Jmol^{-1} from Hultgren et al. [39]). Therefore, once again only the results based on 3rd-law method, $\Delta_f H^{\circ}_{298,\ 3rd}(i)$, are recommended for further application.

5. Discussion

The results obtained via KEMS for the different thermodynamic quantities, such as $\Delta_r H^{\circ}_{298,\ 3rd}$ or $\Delta_f H^{\circ}_{298}(i)$, exhibit deviations within error (~2% relative) of corresponding literature values. These deviations are related to the conversion between measured ion intensity, I_i, into the corresponding partial pressure, p_i, that requires estimation of an additional six factors (*cf.* eq. (4)), some of which are subject to significant uncertainties for different KEMS devices, most notably, cross sections and fragmentation corrections. These uncertainties manifest as relatively large systematic errors on p_i, such as $p(In_2O) = 1.41 \pm 0.52$ Pa at 1611 K (±37%). However, it should be noted that this error marks already a significant improvement in comparison to the average error of 50% reported in Gomez et al. [9] and furthermore becomes small relative to the order-of-magnitude changes in p_i resulting from varying T. The determined p_i and their errors propagate into the calculation of all other thermodynamic quantities. Together, these factors lead to the differences observed between various data sets. In the following sections, possible sources for these discrepancies are identified and evaluated. Furthermore, it is explained how this work improves on the accuracy and precision of the existing data.

5.1. Material of the Knudsen cell

The choice of the material of the Knudsen cell is crucial, since chemical reactions between the sample and cell material can perturb the presumed chemical equilibria (Tables 8–9). While alumina and platinum cells have been used [8,9], Smirnov et al. [10] used quartz effusion cells and emphasise "that the use of platinum or iridium cells is not appropriate due to the ability of platinum metal to dissolve easily most metals to form intermetallides or solid solutions". However, according to the XRD analysis of the residues from the Ir cell used in our experiments after heating (Appendix), there is no indication of any mutual reaction between cell material and sample, whereas XRD and μXRF investigations of the inner cell surface of the quartz cell used by Smirnov et al. [10] showed the presence of $In_2Si_2O_7$. Dissolution of SiO_2 into In_2O_3 would reduce the activity of In_2O_3, such that p_i in the experiments of Smirnov et al. [10] would be expected to be lower than those reported herein. As

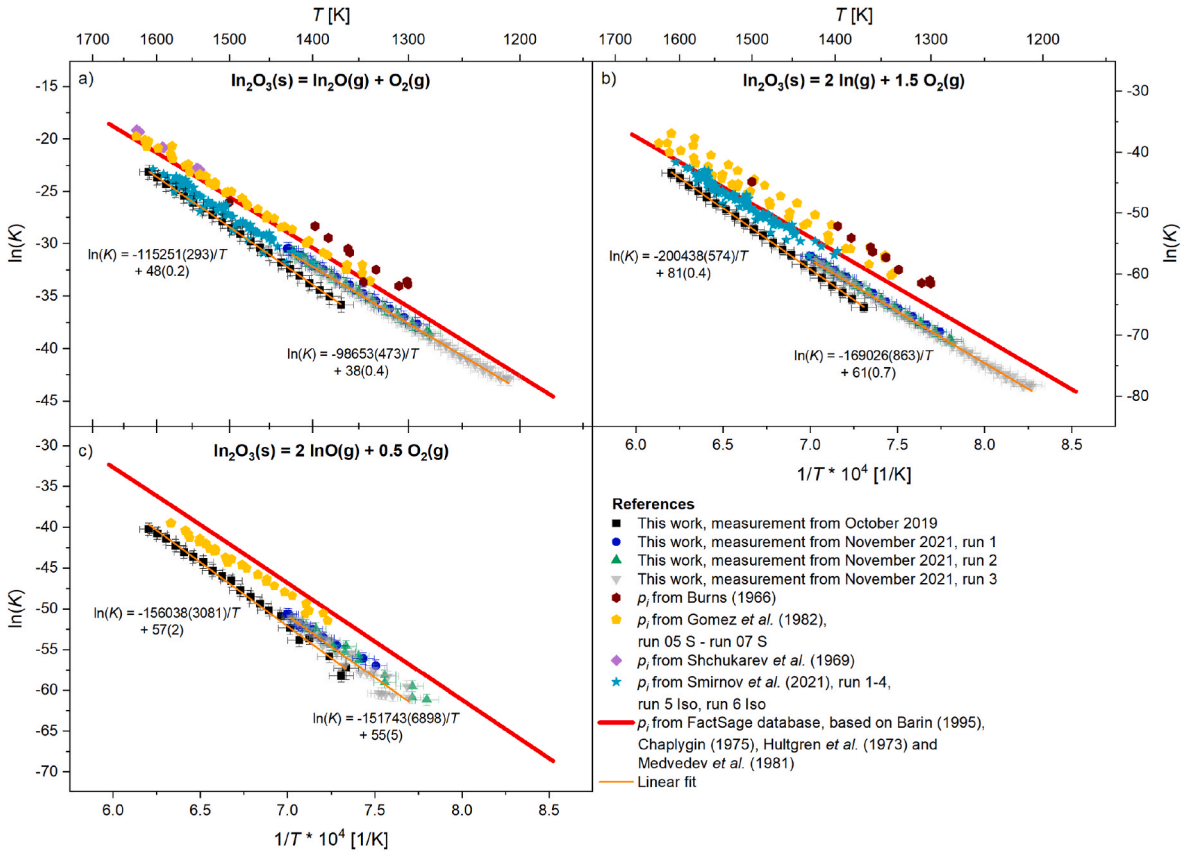

Fig. 8. ln(K) for the reactions of In_2O_3 into a) In_2O, b) In and c) InO plotted *vs.* reciprocal T for measured and literature data.

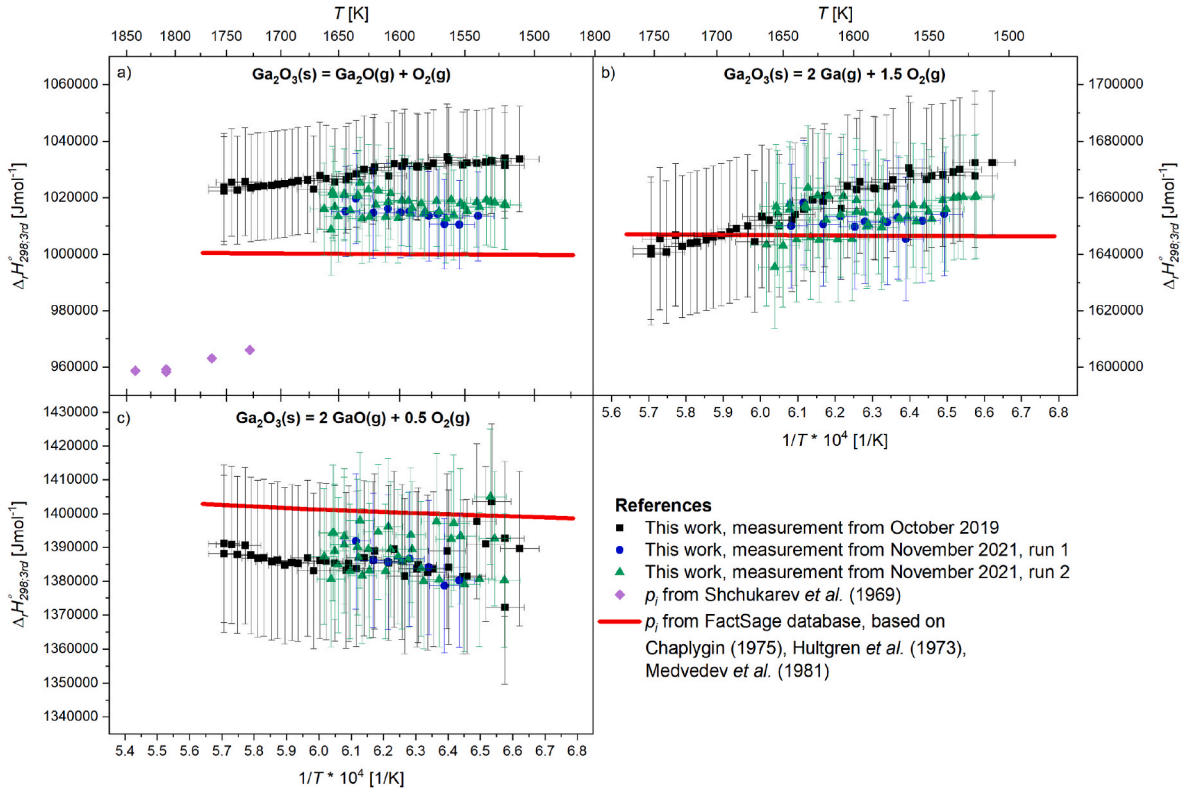

Fig. 9. $\Delta_r H^{o}_{298,3rd}$ for the reactions of Ga_2O_3 into a) Ga_2O, b) Ga and c) GaO plotted *vs.* reciprocal T for measured and literature data.

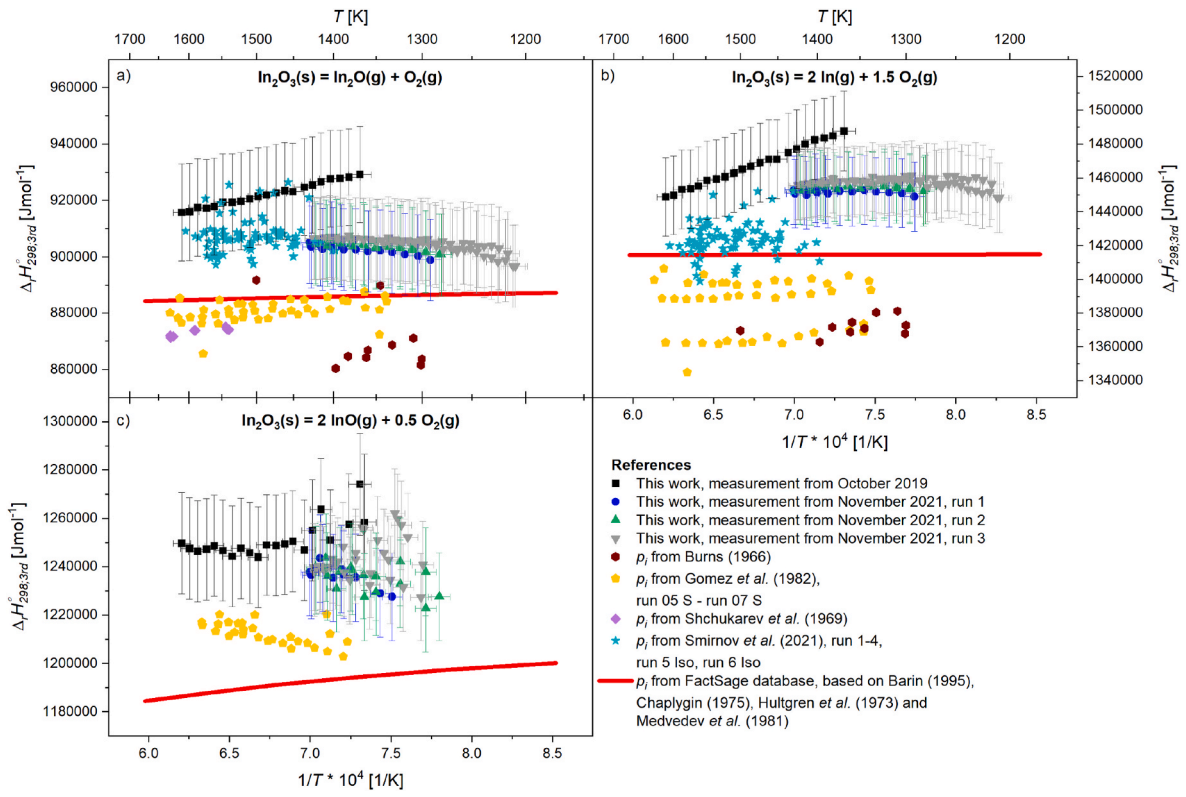

Fig. 10. $\Delta_r H^{\circ}_{298,3rd}$ for the reactions of In_2O_3 into a) In_2O, b) In and c) InO plotted *vs.* reciprocal *T* for measured and literature data.

shown in Table 11, the opposite is observed, indicating that the reaction $In_2O_3 + 2\ SiO_2 = In_2Si_2O_7$ did not result in any resolvable change in p_i. Nevertheless, and contrary to Smirnov et al. [10], we consider Ir cells the most appropriate for the examination of vapour phase reactions above In_2O_3(s).

5.2. Fragmentation correction

Electron-impact ionisation leads to fragmentation, hence a particular ion may also result from various parent molecules (section 3.1). The most unambiguous method of determining the fragmentation efficiency is to measure the intensity I_i of M^+ and M_2O^+ above a mixture of pure metal and metal oxide M-M_2O_3 as carried out and described in detail by Smirnov et al. [10] for In–In_2O_3. The profiles of the ionisation efficiency curves measured here permit a direct quantitative apportioning of the measured signal for $\sum M^+$ to the M atom or the M_2O molecule, respectively, for both, Ga and In (Figs. 2 and 3). The ratio found for In^+/In_2O^+ of 0.19 ± 0.1, which is applied as correction factor *f* (*cf.* section 3.1), is in good agreement with the value of ~0.15 given in Fig. 2 of Smirnov et al. [10]. Consequently, discrepancies in the two studies cannot be ascribed to different fragmentation rates.

5.3. Ionisation cross sections

As shown in Tables 4 and 5, there is a broad range of ionisation cross sections available in the literature. To represent this variety, we took an average of all values available, leading to ionisation cross sections of *e.g.* $\sigma\ (In^+) = 9.74\ Å^2$; $\sigma\ (InO^+) = 7.5\ Å^2$; $\sigma\ (In_2O^+) = 16.03\ Å^2$ and $\sigma(O) = 1.6\ Å^2$. These values differ significantly from those applied in Smirnov et al. [10] ($\sigma\ (In^+) = 6.23\ Å^2$; $\sigma\ (In_2O^+) = 10.22\ Å^2$ and $\sigma(O) = 1.17\ Å^2$). The difference in cross sections may lead to deviations of up to 56% in the calculated partial pressures, causing an upwards revision of the values reported herein (*e.g.*, *p*(In) = 0.30 Pa to *p*(In) = 0.47 Pa at 1610 K) and is the main reason as to why Smirnov et al. [10] obtain higher partial pressures (*e.g.* *p*(In) = 0.62 Pa at 1610 K). These authors take $\sigma\ (In^+)$ from Kim and Stone [28], a study we also include for the calculation of our average σ_i (*cf.* Table 5). However, we use $\sigma\ (In^+) = 11.57\ Å^2$ from Kim and Stone [28], which is the cross section for total counting ionisation. This estimate accounts for the autoionisation of other excitable transitions in the atom based on a model that clearly fits the experimental data shown in their Fig. 4, and is the value the authors recommend for further application. The value of $\sigma\ (In^+) = 6.23\ Å^2$ that Smirnov et al. [10] cite reflects only direct ionisation calculated using the binary-encounter-Bethe (BEB) model. The BEB model provides an incomplete reflection of the true ionisation behaviour, as shown by a clear mismatch between cross sections predicted using this method and experimental results. Additional comparisons of σ_i are not possible, as all other studies do not give the values that were used.

5.4. Temperature calibration

Temperature calibration by optical pyrometry (section 3.1) has a precision of ±0.15% relative at the temperatures covered in the experiments. The linear trends of the natural logarithm of partial pressure with reciprocal temperature indicate that random errors associated with temperature are negligible. The larger scatter in intensities at low temperatures is due to poor ion counting statistics, rather than to the precision of temperature measurements. By contrast, a displacement in linear trends of ln(*p*) with 1/*T* from run to run can frequently be seen in this work or in other studies (*e.g.* [9]) indicative of systematic errors. In this study, temperature is determined through a sighting hole that targets a cavity in the Knudsen cell assembly, with geometrical properties (length/radius = 10) such that the emitted light approaches the behaviour of a black body [22]. Any offset of the measured pyrometer temperature from the cavity and the true temperature inside the cell (*e.g.*, by condensation of high temperature vapours on the sighting windows) are corrected for by the measurement of pure Ag and Ni

Table 9
Summary of the thermodynamic quantities calculated from the measurements carried out within the framework of this study as well as from partial pressures given in literature for reactions involving In-bearing species. Values in parentheses are the original results the corresponding authors calculated from p_i with their own method and thermodynamic data.

T_{mean} [K]	$\Delta_r H^{\circ}_{T,\ 2nd}$ [Jmol^{-1}]	$\Delta_r S^{\circ}_{T,\ 2nd}$ [Jmol^{-1}K^{-1}]	$\Delta_r H^{\circ}_{298,\ 2nd}$ [Jmol^{-1}]	$\Delta_r H^{\circ}_{298,\ 3rd}$ [Jmol^{-1}]	Ref.
$In_2O_3(s) = 2\ In(g) + 1.5\ O_2(g)$					
1487 ± 14	1666682 ± 28944	674 ± 20	1707825 ± 30070	1467405 ± 23300	Oct19
1373 ± 11	1399715 ± 29390	505 ± 22	1437190 ± 30076	1451628 ± 20247	Nov21#1
1351 ± 11	1415181 ± 27652	514 ± 21	1452331 ± 28439	1454254 ± 20296	Nov21#2
1315 ± 11	1404648 ± 26403	504 ± 21	1440698 ± 27467	1457213 ± 20395	Nov21#3
			1509511 ± 132368	1457625 ± 6908	*Mean*
1423	1377337	515	1415766	1414627	Hult73
1482	1337539	506	1378189	1388970 (1402000 ± 8000)	Gom82#1
1489	1352650	509	1393544	1399461 (1383000 ± 17000)	Gom82#2
1486	1393299	561	1434037	1362998 (1402000 ± 23000)	Gom82#3
1359	1385804	553	1424123	1371959	Burns66
1507	1575788 (1573500 ± 85600)	631	1617476 (1602700 ± 85600)	1438858 (1419500 ± 2700)	Smi21#1
1504	1282557 (1282700 ± 45700)	444	1324073 (1312100 ± 45700)	1426671 (1407500 ± 1500)	Smi21#2
1499	1350299 (1345700 ± 25400)	491	1391659 (1374900 ± 25400)	1423711 (1404500 ± 900)	Smi21#3
1504	1394441 (1395900 ± 28900)	522	1436167 (1425200 ± 28900)	1421751 (1402700 ± 1200)	Smi21#4
1540	1382025 (1379800 ± 53100)	516	1424735 (1410100 ± 53100)	1418591 (1399200 ± 900)	Smi21#5
1539	1244192	433	1286817	1408548 (1391000 ± 2300)	Smi21#6
			(1388900 ± 71700)	(1404700 ± 61800)	Smi22
$In_2O_3(s) = 2\ InO(g) + 0.5\ O_2(g)$					
1486 ± 14	1297097 ± 45078	475 ± 31	1351359 ± 45967	1251024 ± 21224	Oct19
1391 ± 11	1018091 ± 54764	290 ± 39	1067405 ± 55434	1236007 ± 18055	Nov21#1
1362 ± 11	1098236 ± 55571	346 ± 41	1146132 ± 56203	1235178 ± 18074	Nov21#2
1368 ± 11	1260565 ± 75634	460 ± 55	1308981 ± 76317	1242901 ± 18132	Nov21#3
			1218469 ± 134046	1241277 ± 7363	*Mean*
1423	1187497	441	1237431	1192479	Barin95
1485	1133161	390	1187309	1212785 (1235000 ± 14000)	Gom82#1
1487	1012563	309	1066157	1212915 (1238000 ± 23000)	Gom82#2
1490	1090894	363	1145540	1211392 (1234000 ± 16000)	Gom82#3
$In_2O_3(s) = In_2O(g) + O_2(g)$					
1487 ± 14	958360 ± 19409	403 ± 13	1006101 ± 20102	922183 ± 17174	Oct19
1373 ± 11	812763 ± 19382	315 ± 14	855864 ± 19938	902583 ± 14467	Nov21#1
1351 ± 11	823264 ± 17816	322 ± 13	865954 ± 18448	903538 ± 14484	Nov21#2
1315 ± 11	819598 ± 17333	318 ± 13	860898 ± 18102	904510 ± 14539	Nov21#3
			897204 ± 72714	908203 ± 9353	*Mean*
1423	850011	354	894318	885837	Chap75
1587	870695	375	922253	873201	Shch69
1488	841062	352	888120	879995 (896000 ± 6000)	Gom82#1
1489	861721	363	909147	883951 (895000 ± 18000)	Gom82#2
1486	880536	380	927766	877772 (901000 ± 10000)	Gom82#3
1359	701119	257	745289	870246	Burns66
1507	888959 (884500 ± 57200)	358	937390 (926800 ± 57200)	918819 (906600 ± 1500)	Smi21#1
1504	820027 (820400 ± 22200)	320	868241 (862800 ± 22200)	907376 (895200 ± 700)	Smi21#2
1499	833791 (836300 ± 10400)	330	881808 (878400 ± 10400)	906220 (894100 ± 400)	Smi21#3
1504	833063 (829800 ± 9000)	329	881542 (872100 ± 9000)	906850 (894800 ± 400)	Smi21#4
1540	918170 (917500 ± 16500)	388	967891 (961200 ± 16500)	901254 (889000 ± 400)	Smi21#5
1539	738508	272	788122	900499 (890400 ± 1800)	Smi21#6
			(877000 ± 55300)	(893200 ± 41900)	Smi22

References.
Barin95: p_i from FACTSAGE database, based on Barin [40].
Burns66: p_i from Burns [23].
Chap75: p_i from FACTSAGE database, based on Chaplygin [37] and Medvedev et al. [38].
Gom82#1–3: p_i from Gomez et al.. [9], run 05 S–07 S.
Hult73: p_i from FACTSAGE database, based on Hultgren et al. [39].
Mean: Mean of the measurements carried out within this work.
Medv81: p_i from FACTSAGE database, based on Medvedev et al. [38].
Nov21#1–3: This work, measurement from November 2021, run 1-3.
Oct19: This work, measurement from October 2019.
Shch69: p_i from Shchukarev et al. [8].
Smi21#1–6: p_i from Smirnov et al. [10], run 1–4, run 5 Iso, run 6 Iso.
Smi22: mean for $\Delta_r H^{\circ}_{298,\ 2nd}$ and $\Delta_r H^{\circ}_{298,\ 3rd}$ from Smirnov et al. [11] for reactions above.
In–In_2O_3, not In_2O_3(s) as in this study.

standards with known melting points. However, because only one Knudsen cell can be loaded at any given time, the geometrical alignment is liable to modification upon sample exchange and tuning. Thermal conditions may thus vary slightly according to the placement of the Knudsen cell, the assembly of heat shields or the position of the pyrometer itself. We conservatively estimate a systematic error of ±5 K that would have a small but significant impact on the derived thermodynamic quantities. Given slopes of ln(p) *vs.* $1/T$ similar for all species (Figs. 5 and 6), ranging from -4.7×10^4 K to -7.0×10^4 K, a systematic offset of 5 K produces an error of ±15% in absolute p_i. However, this

Table 10
$\Delta_f H^{\circ}_{298,\ 2nd}(i)$ and $\Delta_f H^{\circ}_{298,\ 3rd}(i)$ calculated for Ga-bearing species. Values in parentheses are the original results the corresponding authors provide in their work.

Reaction	$\Delta_f H^{\circ}_{298,\ 2nd}(\mathrm{Ga(g)})$ [Jmol^{-1}]	$\Delta_f H^{\circ}_{298,\ 3rd}(\mathrm{Ga(g)})$ [Jmol^{-1}]	Ref.
$Ga_2O_3(s) = 2\,Ga(g) + 1.5\,O_2$ (g)	395078 ± 17705	283695 ± 12636	Oct19
	268912 ± 35584	281335 ± 10948	Nov21#1
	332194 ± 26692	282383 ± 10975	Nov21#2
	332061 ± 63083	282471 ± 1183	*Mean*
	276789	278827	Hult73
Reaction	$\Delta_f H^{\circ}_{298,\ 2nd}(\mathrm{GaO(g)})$ [Jmol^{-1}]	$\Delta_f H^{\circ}_{298,\ 3rd}(\mathrm{GaO(g)})$ [Jmol^{-1}]	Ref.
$Ga_2O_3(s) = 2\,GaO(g) + 0.5\,O_2$ (g)	149195 ± 20299	148776 ± 11505	Oct19
	43317 ± 31645	147843 ± 9962	Nov21#1
	153726 ± 31156	149829 ± 9989	Nov21#2
	115412 ± 62478	148816 ± 993	*Mean*
	144274	155824	Medv81
$GaO(g) = Ga(g) + O$ (g)	129404		Pets04, FACTSG
Reaction	$\Delta_f H^{\circ}_{298,\ 2nd}(\mathrm{Ga_2O(g)})$ [Jmol^{-1}]	$\Delta_f H^{\circ}_{298,\ 3rd}(\mathrm{Ga_2O(g)})$ [Jmol^{-1}]	Ref.
$Ga_2O_3(s) = Ga_2O(g) + O_2$ (g)	16763 ± 24064[a]	−60564 ± 18878	Oct19
	−161061 ± 42543	−74727 ± 15903	Nov21#1
	−82248 ± 34832	−71608 ± 16009	Nov21#2
	−121654 ± 55729	−68966 ± 7442	*Mean*
	−93315	−88996	Chap75
	3116	−128077 (−87860)	Shch69

References.
Chap75: p_i from FACTSAGE database, based on Chaplygin [37] and Medvedev et al. [38].
FACTSG: $\Delta_f H^{\circ}_{298}(i)$ calculated from FACTSAGE.
Hult73: p_i from FACTSAGE database, based on Hultgren et al. [39].
Medv81: p_i from FACTSAGE database, based on Medvedev et al. [38].
Nov19#1–2: This work, measurement from November 2019, run 1-2.
Oct19: This work, measurement from October 2019.
Pets04: Petsalakis et al. [41].
Shch69: Shchukarev et al. [8].
[a] Excluded from the calculation of the mean.

shift affects all species in the same manner, the propagated uncertainty on K is significantly smaller, *i.e.* < 0.5% on calculated values of $\Delta_r H^{\circ}_{298,\ 3rd}$. This magnitude often corresponds to the offset between this work and that of Smirnov et al. [10] for In. Yet, 0.5% is much smaller than differences to earlier KEMS work by Gomez et al. [9] and Burns [23] for In, and by Shchukarev et al. [8] for In and Ga, these are typically 2–5%.

5.5. Partial pressure of O_2

The partial pressure of oxygen, $p(O_2)$, which is needed for the calculation of K (*cf.* eq. (19)), is not easily quantified by KEMS owing to a relatively high signal/background ratio of O_2. As a result, it was calculated by considering the congruent vaporisation of individual reactions involving metal-bearing gases (section 3.1, Table 5). Smirnov et al. [10] take a different mathematical approach, based on the same assumption that In_2O_3 evaporates congruently, such that the molar ratio of In and O in the vapour is that of the condensed phase, that is, In/O = 2/3. The outcome at two different temperatures is listed in Table 12. Since single partial pressures do not allow a robust comparison between different measurements (*cf.* section 4.3.2), the ratio between the partial pressures of In-bearing species and oxygen are also listed.

Despite the differing approaches, $p(O_2)$ calculated by Smirnov et al. [10] when compared to (p(In) + $p(In_2O)$), is indistinguishable from ours. Rather, differences are evident in the *i*) absolute partial pressures and *ii*) In/In_2O ratio. As shown in section 5.3, different absolute partial pressures are explained by the use of lower cross sections by Smirnov et al. [10]. Deviations with regard to In/In_2O ratios can neither result from different cross sections nor from different fragmentation corrections (section 5.2), but likely derive from different $p(O_2)$ within the cell, possibly due to the contribution of O_2 evaporating from the quartz cell in the experiments of Smirnov et al. [10]. Since $p(O_2)$ is always in the numerator of the equilibrium constant, this process may explain why the values of K determined by Smirnov et al. [10] are systematically higher than ours at a given temperature (Fig. 8). The fact that the difference in the M/O_2 ratios is much higher for In (~55%) than for In_2O (~25%) could explain why the datasets for K(In_2O) match much better than those for K(In) from In_2O_3 in Fig. 8.

5.6. Influence of the MO species and comparison with ab initio studies

Homogeneous gas phase equilibria, notably eq. (32), enables an independent estimation of data quality independent of $p(O_2)$. Plots of ln (K) and $\Delta_r H^{\circ}_{298,\ 3rd}$ *vs.* T for these reactions are shown in Fig. 11 and highlight the precision of our measurements. The resulting thermodynamic data is summarised in Table 13.

$$M_2O(g) = M(g) + MO(g) \quad (32)$$

It is noteworthy that the values obtained for $\Delta_r H^{\circ}_{298,\ 3rd}$ of eq. (30) in this work and those of Gomez et al. [9] on In converge to a common value around 440000 Jmol^{-1} at higher temperatures at which the precision of the determined partial pressures are not limited by the poor counting statistics on InO(g). Deviation of our estimates from FACTSAGE are of the order of 4% relative, larger than for the corresponding vaporisation reactions owing to the compounding discrepancy of the vaporisation reactions involving Ga_2O(g) and GaO(g). Answers to the question of the origin of MO are contradictory [10]. While Lynch [43] states that all the MO^+ derives from fragmentation of M_2O, for both Ga and In, based on his measurements of appearance potentials above M-M_2O_3, Gomez et al. [9] infer from their measurements of appearance potentials above pure In_2O_3 that fragmentation of In_2O into In^+ is much more favourable than into InO^+, *i.e.* that the precursor of InO^+ is InO from In_2O_3(s). Given that within this work the gas phase above the pure oxides M_2O_3 is investigated, Gomez et al. [9] was taken as a benchmark and InO^+ was assigned to InO from In_2O_3. Nevertheless, the opposite case is briefly examined below. Should fragmentation of M_2O into MO^+

Table 11
$\Delta_f H^{\circ}_{298,\ 2nd}(i)$ and $\Delta_f H^{\circ}_{298,\ 3rd}(i)$ calculated for In-bearing species. Values in parentheses are the original results the corresponding authors provide in their work.

Reaction	$\Delta_f H^{\circ}_{298,\ 2nd}(\mathrm{In(g)})$ [Jmol^{-1}]	$\Delta_f H^{\circ}_{298,\ 3rd}(\mathrm{In(g)})$ [Jmol^{-1}]	Ref.
$In_2O_3(s) = 2\ In(g) + 1.5\ O_2(g)$	391018 ± 15035	270808 ± 11650	Oct19
	255700 ± 15038	262920 ± 10124	Nov21#1
	263271 ± 14220	264232 ± 10148	Nov21#2
	257455 ± 13734	265712 ± 10198	Nov21#3
	291861 ± 66184	265918 ± 3454	*Mean*
	244988	244419	Hult73
	226200	231590	Gom82#1
	233878	236836	Gom82#2
	254124	218604	Gom82#3
	249167	223085	Burns66
	345843	256534	Smi21#1
	199142	250441	Smi21#2
	232935	248961	Smi21#3
	255189	247981	Smi21#4
	249473	246401	Smi21#5
Reaction	$\Delta_f H^{\circ}_{298,\ 2nd}(\mathrm{InO(g)})$ [Jmol^{-1}]	$\Delta_f H^{\circ}_{298,\ 3rd}(\mathrm{InO(g)})$ [Jmol^{-1}]	Ref.
$In_2O_3(s) = 2\ InO(g) + 0.5\ O_2$ (g)	212785 ± 22983	162618 ± 10612	Oct19
	70808 ± 27717	155109 ± 9028	Nov21#1
	110172 ± 28101	154694 ± 9037	Nov21#2
	191596 ± 38158	158556 ± 9066	Nov21#3
	146340 ± 67023	157744 ± 3681	*Mean*
	155821	133345	Barin95
	130760	143498	Gom82#1
	70184	143563	Gom82#2
	109875	142801	Gom82#3
$InO(g) = In(g) + O$ (g)	158014		Mukh10, FACTSG
Reaction	$\Delta_f H^{\circ}_{298,\ 2nd}(\mathrm{In_2O(g)})$ [Jmol^{-1}]	$\Delta_f H^{\circ}_{298,\ 3rd}(\mathrm{In_2O(g)})$ [Jmol^{-1}]	Ref.
$In_2O_3(s) = In_2O(g) + O_2$ (g)	80312 ± 20102[a]	−3606 ± 17174[a]	Oct19
	−69925 ± 19938	−23206 ± 14467	Nov21#1
	−59835 ± 18448	−22251 ± 14484	Nov21#2
	−64891 ± 18102	−21279 ± 14539	Nov21#3
	−64884 ± 5045	−22245 ± 964	*Mean*
	−31471	−39952	Chap75
	−3536	−52588	Shch69
	−37669	−45794 (−15200 ± 7000)	Gom82#1
	−16642	−41838 (−15200 ± 7000)	Gom82#2
	1977	−48017 (−15200 ± 7000)	Gom82#3
	−180500	−55543 (22100 ± 16700)	Burns66
	11601	−6970 (−33200 ± 12900)	Smi21#1
	−57548	−18413 (−33200 ± 12900)	Smi21#2
	−43981	−19569 (−33200 ± 12900)	Smi21#3
	−44247	−18939 (−33200 ± 12900)	Smi21#4
	42102	−24535 (−33200 ± 12900)	Smi21#5
	−137667	−25290 (−33200 ± 12900)	Smi21#6
		(-31300 ± 8700)	Smi22

References.
Barin95: p_i from FACTSAGE database, based on Barin [40].
Burns66: p_i from Burns [23].
Chap75: p_i from FACTSAGE database, based on Chaplygin [37] and Medvedev et al. [38].
FACTSG: $\Delta_f H^{\circ}_{298}(i)$ calculated from FACTSAGE.
Gom82#1–3: p_i from Gomez et al.. [9], run 05 S–07 S.
Hult73: p_i from FACTSAGE database, based on Hultgren et al. [39].
Medv81: p_i from FACTSAGE database, based on Medvedev et al. [38].
Mukh10: Mukhopadhyay et al. [42].
Nov19#1–3: This work, measurement from November 2019, run 1-3.
Oct19: This work, measurement from October 2019.
Shch69: p_i from Shchukarev et al. [8].
Smi21#1–6: p_i and $\Delta_f H^{\circ}_{298,\ 3rd}(\mathrm{In_2O(g)})$ from Smirnov et al. [10], run 1–4, run 5 Iso, run 6 Iso.
Smi22: mean value for $\Delta_f H^{\circ}_{298,\ 3rd}(\mathrm{In_2O(g)})$ from Smirnov et al. [11].
[a] Estimated as an outlier using the Grubbs test and excluded from calculation of the recommended value.

have occurred, a correction of $p(M_2O)$ by adding the measured $p(MO)$ would be required. This would result in an increase of $p(Ga_2O) = 0.79 \pm 0.3$ Pa at 1752 K to $p(Ga_2O + GaO) = 0.80 \pm 0.3$ Pa at 1752 K, which corresponds to ~1%, as well as of $p(In_2O) = 1.41 \pm 0.52$ Pa at 1611 K to $p(In_2O + InO) = 1.42 \pm 0.52$ Pa at 1611 K, *i.e.* ~0.3%. However, the change in ln(K) would be negligible. Thus, whether MO originates as product from M_2O(g) fragmentation or from direct vaporisation from M_2O_3(s) does not affect the $\Delta_r H^{\circ}_{298,\ 3rd}$ and $\Delta_f H^{\circ}_{298,\ 3rd}$ of M_2O(g) in any resolvable manner.

Whether MO(g) is a primary product of vaporisation or not can be tested independently by comparing thermodynamic data derived herein with those from *ab initio* studies. The bonding energies of 4.06 eV for GaO and 3.48 eV for InO related to the reaction $MO(g) = M(g) + O$ (g) calculated by Petsalakis et al. [41] and Mukhopadhyay et al. [42], respectively,

Table 12
Comparison of partial pressures of In, In_2O, O_2 and their ratios at 1425 and 1550 K for data obtained from this work (Oct. 2019) and taken from Smirnov et al. [10], run 1.

T [K]	1425		1550	
References	This work, Oct. 2019	Smirnov et al. [10], run 1	This work, Oct. 2019	Smirnov et al. [10], run 1
p(In) [Pa]	0.003	0.008	0.072	0.192
$p(In_2O)$ [Pa]	0.014	0.017	0.327	0.376
$p(O_2)$ [Pa]	0.006	0.009	0.147	0.212
p(In)/$p(In_2O)$	0.23	0.47	0.22	0.51
p(In)/$p(O_2)$	0.51	0.89	0.49	0.91
$p(In_2O)/p(O_2)$	2.22	1.89	2.23	1.77
$p(In + In_2O)/p(O_2)$	2.72	2.78	2.72	2.68

result in $\Delta_f H^o_{298}(GaO(g)) = 129404$ Jmol^{-1} and $\Delta_f H^o_{298}(InO(g)) = 158014$ Jmol^{-1}, when calculating from $\Delta_f H^o_{298}(Ga(g)) = 271960$ Jmol^{-1}, $\Delta_f H^o_{298}(In(g)) = 244609$ Jmol^{-1} and $\Delta_f H^o_{298}(O(g)) = 249173$ Jmol^{-1} (*cf.* section 4.3.4). $\Delta_f H^o_{298,\ 3rd}(GaO(g)) = 148816 \pm 993$ Jmol^{-1} found herein exhibits thus a deviation of ~15%, whereas $\Delta_f H^o_{298,\ 3rd}(InO(g)) = 157744 \pm 3681$ Jmol^{-1} is in excellent agreement with the theoretical value (~0.2%). The good agreement of theoretical and experimental results support a primary origin for MO(g) above the sesquioxides. In any case, our results are much closer to the theoretical values than any previous study (*cf.* Tables 10 and 11) and suggest an adjustment of the thermodynamic constants in the FACTSAGE database for these species.

5.7. Data sets applied

In this work, in order to provide a common reference for comparison, all thermodynamic quantities reported in literature were recalculated using the raw partial pressures reported in the individual references. However, as discussed, the reported partial pressures are already subject to significant uncertainties, which include, but are not limited to the ionisation cross sections and $p(O_2)$. Gomez et al. [9] quantify the uncertainty of their partial pressures as follows: "Taking into account the calibration problems, the absolute values are given to within about ±50%".

Data sources for Ga and In FACTSAGE are given as Hultgren et al. [39]; Chaplygin [37]; Medvedev et al. [38] and Barin [40]. With the exception of Chaplygin [37], these are data collections, not original studies. Since Hultgren et al. [39] and Medvedev et al. [38] are not readily accessible, data collection methods and quality remain unknown. Barin [40] refers to the IVTANTHERMO database as well as to Chaplygin [37] (*cf.* [10]; and references therein). Neither of these are accessible either, but Smirnov et al. [10] state, that Chaplygin [37] obtained their data by means of the flow (*i.e.*, transpiration) method using a reaction of liquid indium and water vapour and assess the quality as rather poor, stating that the value for the enthalpy of reaction "is quite different from the mean of the enthalpies from IVTANTHERMO and moreover lies outside the confidence interval of the mean". Smirnov et al. [10] note that "Other available reference books refer to the IVTANTHERMO, or to each other." Thus, we contend that the experimental results for In_2O_3 vaporisation of Smirnov et al. [10] are the most reliable reference for comparison of *K*. Discrepancies observed with respect to $\Delta_r H^o_{298,\ 3rd}$ (up to ~5% relative) and $\Delta_f H^o_{298,\ 3rd}(i)$ (up to ~33% relative) are mainly attributed to the different ionisation cross sections applied, with minor additional uncertainties arising from the choice of cell material and the temperature calibration. The extent of the differences that arise from the reported p_i to calculation of $\Delta_r H^o_{298,3rd}$ and $\Delta_f H^o_{298,3rd}(i)$ alone can be seen in Tables 9–12. Concerning $\Delta_r H^o_{298,\ 3rd}$, a further reason for the discrepancies of up to ~5% is the use of different Gibbs energy functions $gef^o_{298}(T)$ and Gibbs energy functions of reaction $\Delta_r gef^o_{298}(T)$, respectively. While Smirnov et al. [10] refer to the IVTANTHERMO database that gives an average value of $\Delta_r gef^o_{298}(T) = -154\ \frac{J}{mol\ K}$ for the reaction $In_2O(g) = 2\ In(g) + 0.5\ O_2\ (g)$ for the temperature range considered (1400–1570 K), we use a value of $-162\ \frac{J}{mol\ K}$ from FACTSAGE. This leads to deviations of up to 8 kJ (2%) for this reaction. Compared to the data from

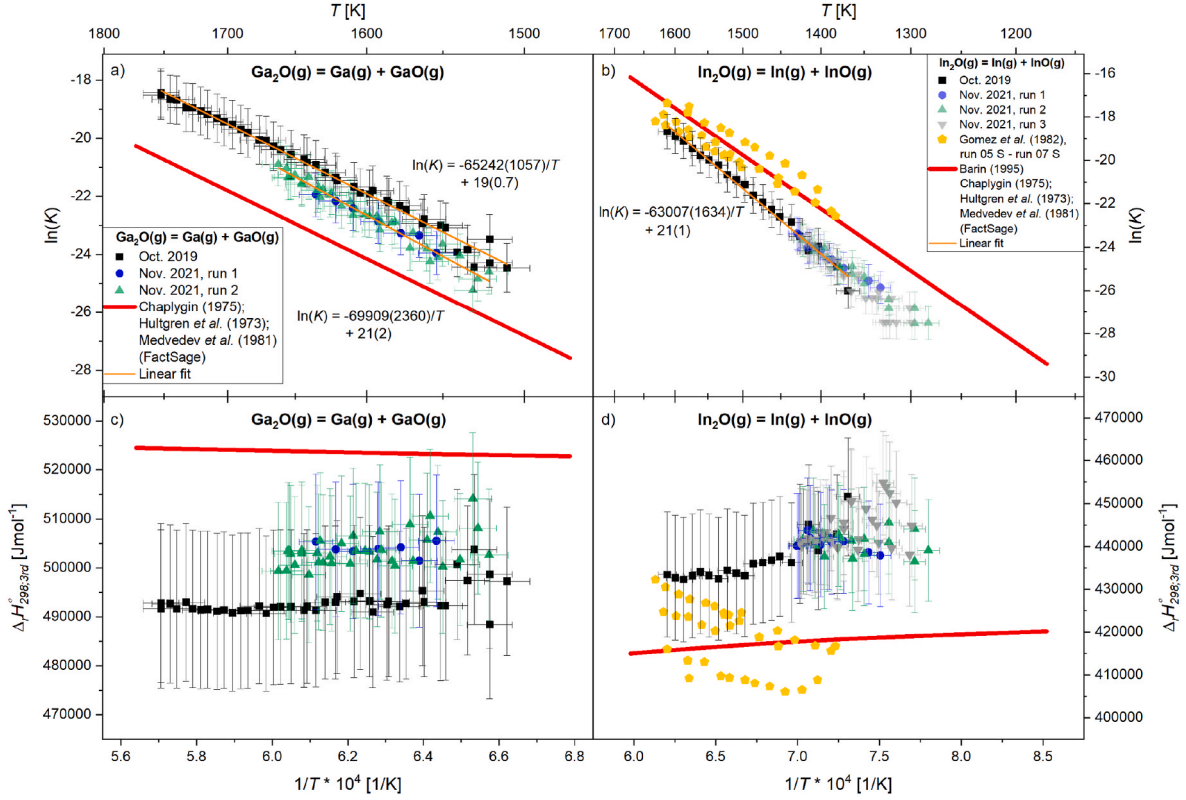

Fig. 11. ln(*K*) and $\Delta_r H^o_{298,3rd}$ plotted *vs.* reciprocal *T* for measured and literature data for the reaction $M_2O(g) = M(g) + MO(g)$ for a), c) Ga and b), d) In.

Table 13
Summary of the thermodynamic quantities calculated from the measurements carried out within the framework of this study as well as from partial pressures given in literature for the reaction $M_2O(g) = M(g) + MO(g)$.

T_{mean} [K]	$\Delta_r H^o_{T,\ 2nd}$ [Jmol^{-1}]	$\Delta_r S^o_{T,\ 2nd}$ [Jmol^{-1}K^{-1}]	$\Delta_r H^o_{298,\ 2nd}$ [Jmol^{-1}]	$\Delta_r H^o_{298,\ 3rd}$ [Jmol^{-1}]	Ref.
$Ga_2O(g) = Ga(g) + GaO(g)$					
1633 ± 14	542657 ± 24745	157 ± 15	527510 ± 24774	493035 ± 15650	Oct19
1593 ± 12	504625 ± 45915	127 ± 29	489914 ± 45857	503932 ± 13667	Nov21#1
1603 ± 12	581236 ± 33920	175 ± 21	566526 ± 33863	503497 ± 13760	Nov21#2
				500155 ± 6169	*Mean*
1623	529329	130	514378	523647	HCM778
$In_2O(g) = In(g) + InO(g)$					
1492 ± 14	524420 ± 28423	172 ± 19	524495 ± 28571	436731 ± 14156	Oct19
1391 ± 11	396127 ± 31171	82 ± 22	395969 ± 31202	440712 ± 12150	Nov21#1
1362 ± 11	433134 ± 31707	108 ± 23	432915 ± 31761	440894 ± 12076	Nov21#2
1368 ± 11	511664 ± 41531	163 ± 30	511467 ± 41593	444169 ± 12123	Nov21#3
				440627 ± 3044	MEAN
1423	432406	124	432280	417716	HCMB95
1514	367789	79	367893	420925	Gom82#1
1526	323659	48	323768	424604	Gom82#2
1508	356004	78	356116	409698	Gom82#3

References.
HCM778: p_i from FACTSAGE database, based on Hultgren et al. [39]; Chaplygin [37]; Medvedev et al. [38].
HCMB95 p_i from FACTSAGE database, based on Hultgren et al. [39]; Chaplygin [37]; Medvedev et al. [38]; Barin [40].
Nov21#1–3: This work, measurement from November 2021, run 1-3.
Oct19: This work, measurement from October 2019.
Gom82#1–3: Gomez et al.. [9], run 05 S–07 S.

Gomez et al. [9] for the reaction mentioned, the magnitude of the discrepancy is the same. They provide no value for $\Delta_r gef^o_{298}(T)$, but only a reference [44] that is not accessible either. When considering $\Delta_f H^o_{298,\ 3rd}(i)$, additional deviations result from the $\Delta_f H^o_{298}(In_2O_3)$ of −925789 Jmol^{-1} used here and −926300 Jmol^{-1} in Smirnov et al. [10], while both are ~0.3% higher than the value recommended by Cordfunke et al. [45]. The value for $\Delta_f H^o_{298,\ 3rd}(In_2O(g)) = -22245 \pm 964$ Jmol^{-1} obtained in this work is in good agreement with the values given in Burns [23] $\Delta_f H^o_{298}(In_2O(g)) = -22100 \pm 16700$ Jmol^{-1} and Gomez et al. [9] $\Delta_f H^o_{298}(In_2O(g)) = -15200 \pm 7000$ Jmol^{-1} as well as the value we calculated from the partial pressures in Smirnov et al. [10] of $\Delta_f H^o_{298,\ 3rd}(In_2O(g)) = -21349 \pm 3289$ Jmol^{-1}, using $gef^o_{298}(T)$ given in FACTSAGE.

Therefore, and considering the error with regard to the cross section (*cf.* section 5.3) as well as the generally poorer precision in the results of Smirnov et al. [10] (*cf.* section 4.3.3, Fig. 10), we propose a value of $\Delta_f H^o_{298,\ 3rd}(In_2O(g)) = -22245 \pm 964$ Jmol^{-1}, rather than −30700 ± 15900 Jmol^{-1} reported in Smirnov et al. [10] or the updated −31300 ± 8700 Jmol^{-1} in Smirnov et al. [11], $\Delta_f H^o_{298,\ 3rd}(In(g)) = 265918 \pm 3454$ Jmol^{-1} and $\Delta_f H^o_{298,\ 3rd}(InO(g)) = 157744 \pm 3681$ Jmol^{-1}. For Ga, the equivalent values are $\Delta_f H^o_{298,\ 3rd}(Ga(g)) = 282471 \pm 1183$ Jmol^{-1}, $\Delta_f H^o_{298,\ 3rd}(Ga_2O(g)) = -68966 \pm 7442$ Jmol^{-1} and $\Delta_f H^o_{298,\ 3rd}(GaO(g)) = 148816 \pm 993$ Jmol^{-1}.

6. Conclusion

Thermodynamic properties for vaporisation reactions above solid Ga_2O_3 and In_2O_3 were quantified by means of KEMS in order to improve determinations given the considerable spread in the existing data. We find that M_2O (where M = Ga or In) is the most abundant vapour species above pure M_2O_3(s), followed by M, and MO, in agreement with literature results. Equilibrium constants K for the vaporisation reactions of Ga_2O_3(s) match the reference values within error (~2% relative) and we propose $\Delta_f H^o_{298,\ 3rd}(Ga(g)) = 282471 \pm 1183$ Jmol^{-1}, $\Delta_f H^o_{298,\ 3rd}(GaO(g)) = 148816 \pm 993$ Jmol^{-1} and $\Delta_f H^o_{298,\ 3rd}(Ga_2O(g)) = -68966 \pm 7442$ Jmol^{-1}, the latter somewhat smaller than the value given so far (−88996 Jmol^{-1}). Thermodynamic quantities determined for the vaporisation reactions of In_2O_3(s) are within uncertainty of those reported by Smirnov et al. [10]. Deviations are ascribed to the application of erroneous ionisation cross sections, different cell material and the temperature calibration, as well as differences in the Gibbs energy functions used from literature. We recommend $\Delta_f H^o_{298,\ 3rd}(In(g)) = 265918 \pm 3454$ Jmol^{-1}, $\Delta_f H^o_{298,\ 3rd}(InO(g)) = 157744 \pm 3681$ Jmol^{-1} and $\Delta_f H^o_{298,\ 3rd}(In_2O(g)) = -22245 \pm 964$ Jmol^{-1}. A comparison with *ab initio* studies for the reaction $MO(g) = M(g) + O(g)$ identifies our results as the closest to the theoretical values so far with a deviation of ~0.2% for $\Delta_f H^o_{298,\ 3rd}(InO(g)) = 157744 \pm 3681$ Jmol^{-1} and highlights the improvement in data achieved within this study.

Declaration of competing interest

The authors declare that they have no known competing financial interests or personal relationships that could have appeared to influence the work reported in this paper.

Data availability

All data shown in figures is provided under "Supplementary data".

Acknowledgements

L.B. and P.A.S. acknowledge support from the Swiss National Science Foundation (SNSF) via Ambizione Fellowship (#180025).

Supplementary data

Supplementary data to this article can be found online at https://doi.org/10.1016/j.calphad.2022.102507.

Appendix

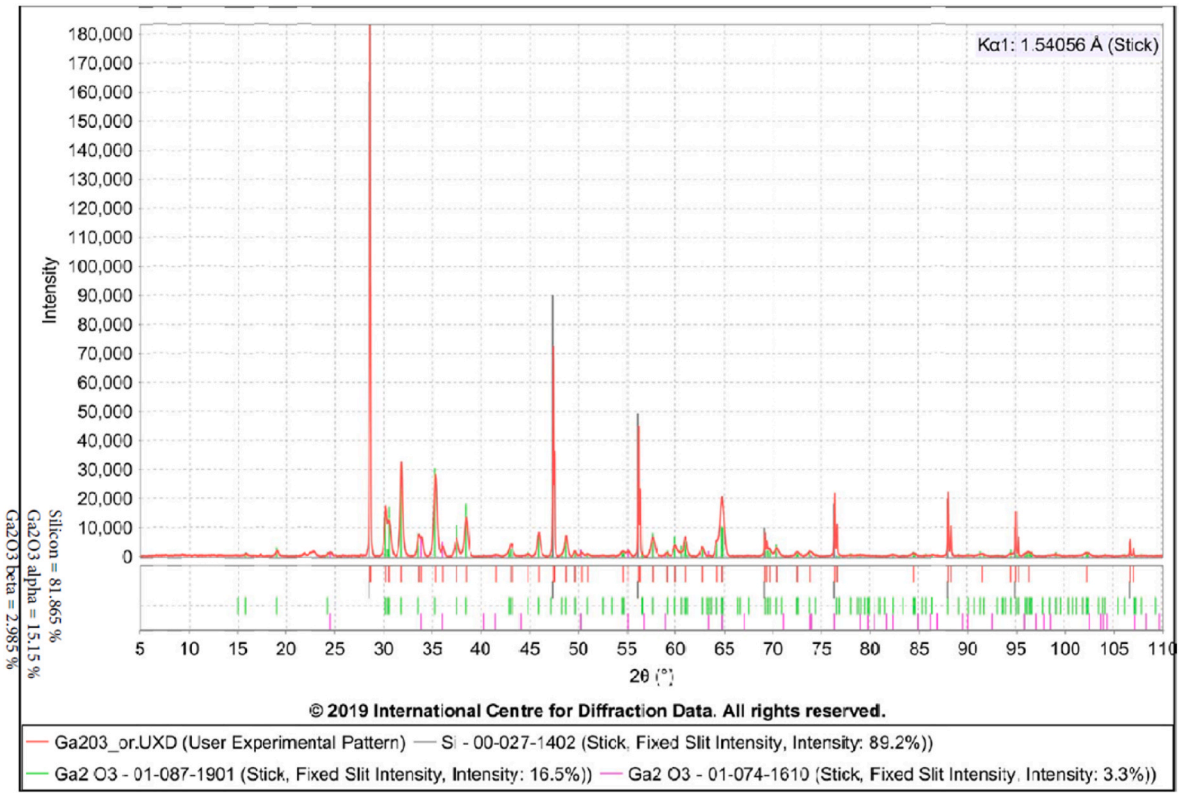

Fig. 12. Structure of Ga_2O_3 before the experiment, mainly α-Ga_2O_3.

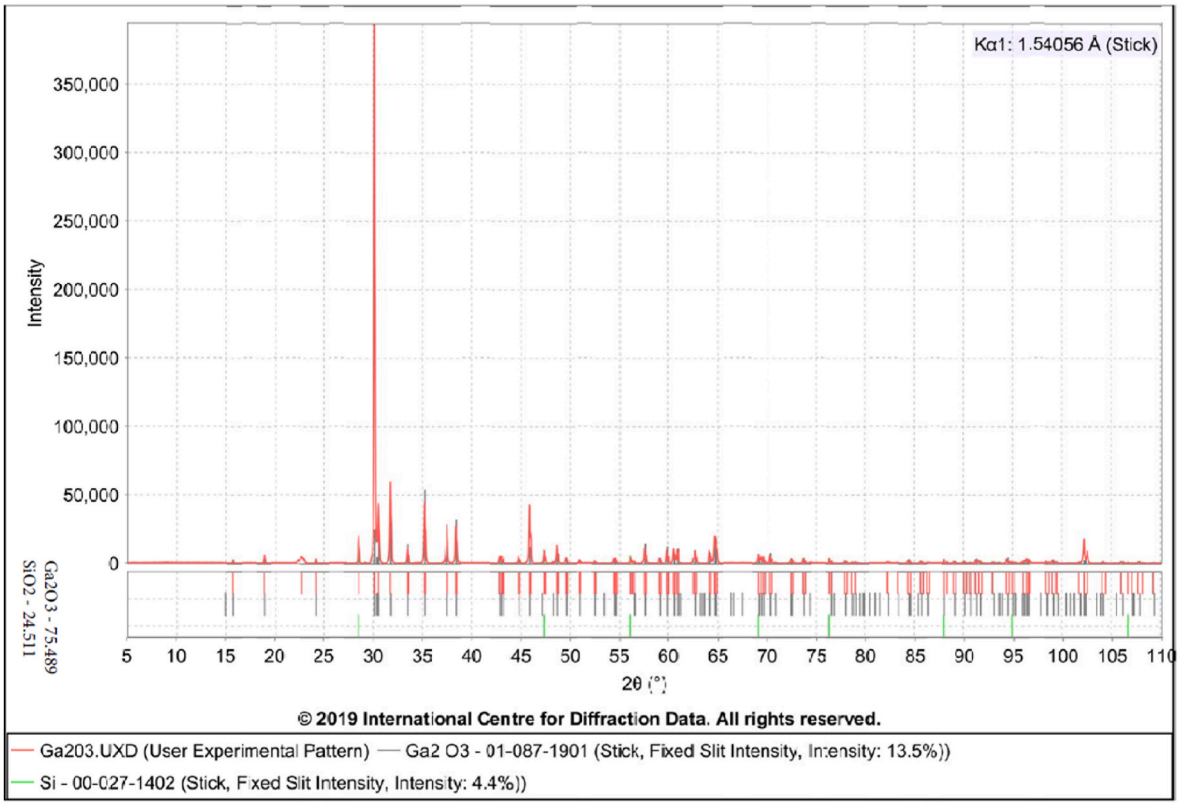

Fig. 13. Structure of Ga_2O_3 after the experiment, mainly β-Ga_2O_3.

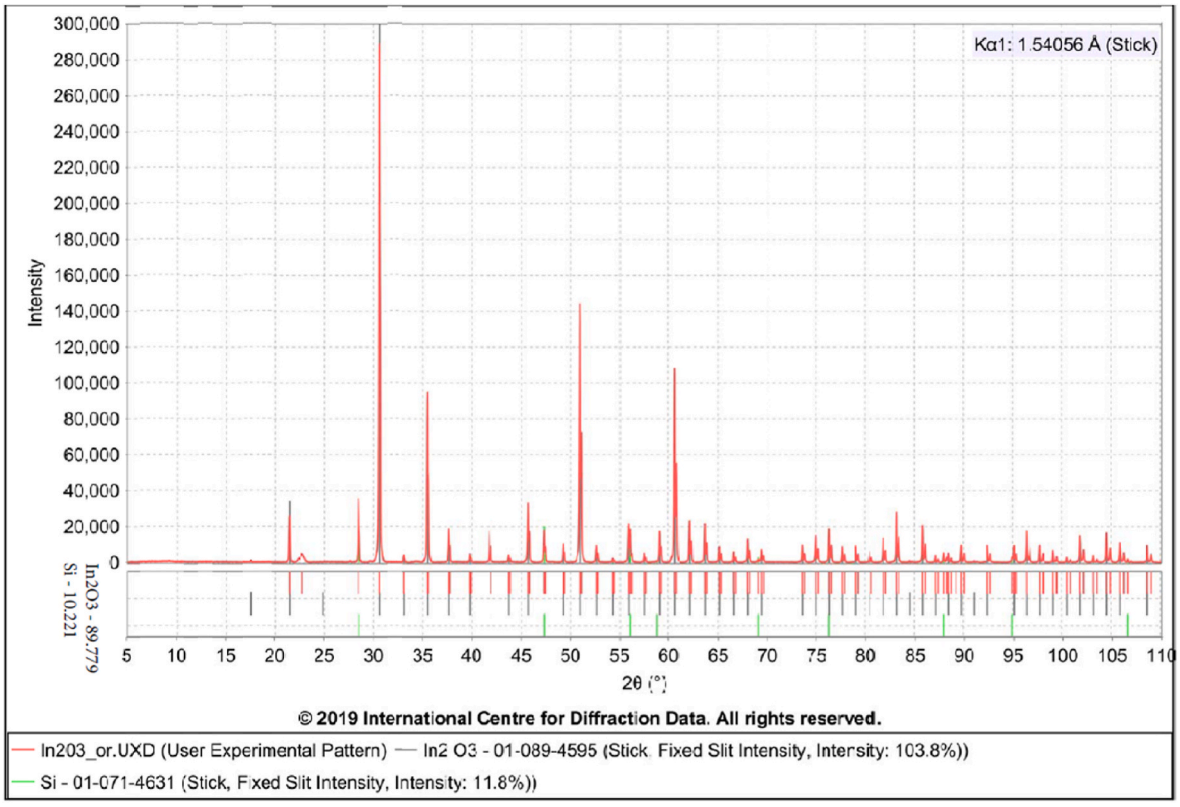

Fig. 14. Structure of In_2O_3 before the experiment.

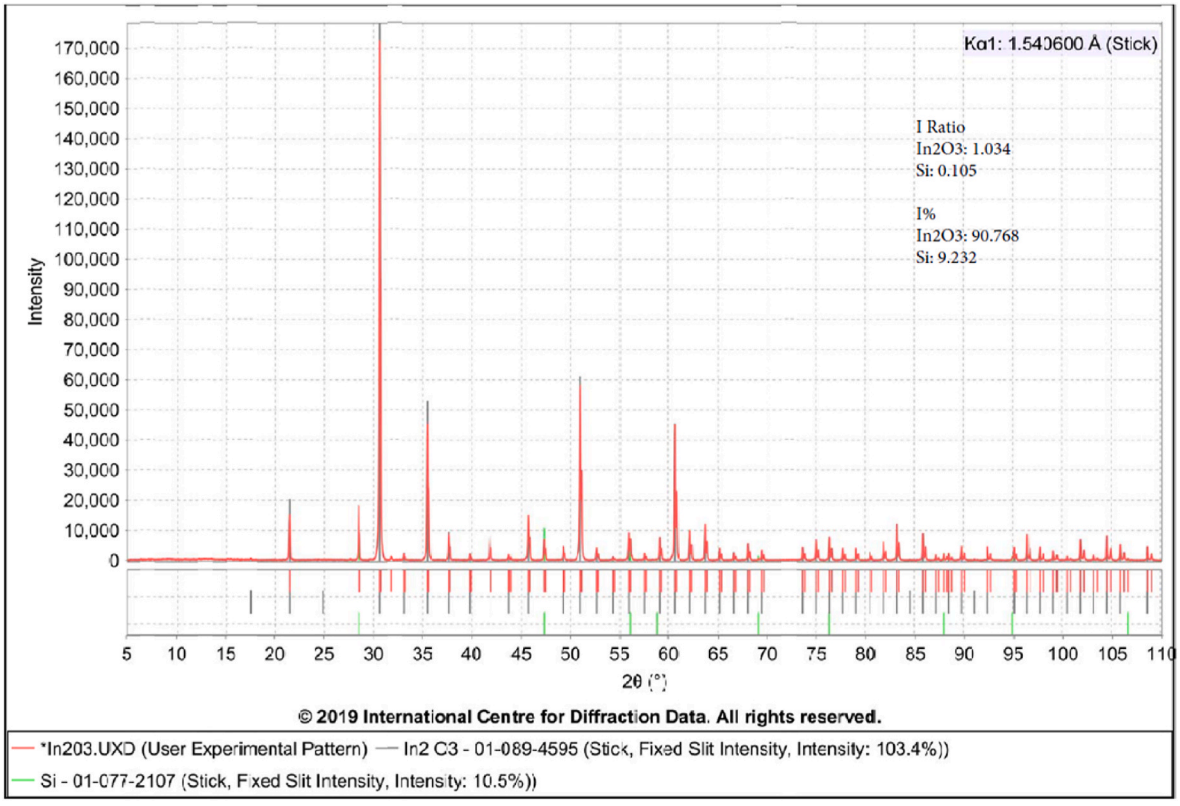

Fig. 15. Structure of In_2O_3 after the experiment.

References

[1] L. Li, W. Wei, M. Behrens, Synthesis and Characterization of α-, β-, and γ-Ga 2o 3 Prepared from Aqueous Solutions by Controlled Precipitation, 14, Solid State Sciences, 2012, pp. 971–981, https://doi.org/10.1016/j.solidstatesciences.2012.04.037.

[2] O. Bierwagen, Indium oxide - a transparent, wide-band gap semiconductor for (opto)electronic applications, Semicond. Sci. Technol. 30 (2015), https://doi.org/10.1088/0268-1242/30/2/024001.

[3] S.I. Stepanov, et al., Gallium oxide: properties and applications - a review, Rev. Adv. Mater. Sci. 44 (2016) 63–86.

[4] R. Roy, V.G. Hill, E.F. Osborn, Polymorphism of Ga2O3 and the system Ga2O3—H2O, J. Am. Chem. Soc. 74 (1952) 719–722.

[5] N.N. Greenwood, The chemistry of gallium, Adv. Inorg. Chem. Radiochem. 5 (1963) 91–134, https://doi.org/10.1016/S0065-2792(08)60153-3.

[6] A.F. Holleman, E. Wiberg, N. Wiberg, Lehrbuch der Anorganischen Chemie, 102nd ed., Walter de Gruyter & Co., Berlin, 2007.

[7] S.Z. Karazhanov, et al., Phase stability, electronic structure, and optical properties of indium oxide polytypes, Phys. Rev. B Condens. Matter 76 (2007) 1–13, https://doi.org/10.1103/PhysRevB.76.075129, 075129.

[8] S.A. Shchukarev, G.A. Semenov, I.A. Rat'kovskii, A thermal investigation of the evaporation of gallium and indium oxides, Russ. J. Inorg. Chem. 14 (1) (1969).

[9] M. Gomez, C. Chatillon, M. Allibert, Thermodynamics of gaseous and condensed indium oxides by mass spectrometry with controlled oxygen pressure, J. Chem. Therm. 14 (1982) 447–459, https://doi.org/10.1016/0021-9614(82)90137-9.

[10] A.S. Smirnov, N.A. Gribchenkova, A.S. Alikhanyan, Vaporization thermodynamics of In2O3 by Knudsen effusion mass spectrometry. The standard enthalpy of formation of In2O(g), Rapid Commun. Mass Spectrom. 35 (15) (2021), https://doi.org/10.1002/rcm.9127.

[11] A.S. Smirnov, N.A. Gribchenkova, A.S. Alikhanyan, Thermodynamics of heterogeneous equilibria in the In–In2O3 system using Knudsen effusion mass spectrometry, Rapid Commun. Mass Spectrom. 36 (2022), https://doi.org/10.1002/rcm.9248.

[12] G.C.C. Costa, N.S. Jacobson, B. Fegley, Vaporization and thermodynamics of forsterite-rich olivine and some implications for silicate atmospheres of hot rocky exoplanets, Icarus 289 (2017) 42–55, https://doi.org/10.1016/j.icarus.2017.02.006.

[13] Z.H. Dong, et al., Vaporization of Ni, Al and Cr in Ni-base alloys and its influence on surface defect formation during manufacturing of single-crystal components, Metall. Mater. Trans. 51 (2020) 309–322, https://doi.org/10.1007/s11661-019-05498-1.

[14] D. Kobertz, M. Müller, A. Molak, Vaporization and caloric studies on lead titanate, Calphad Comput. Coupling Phase Diagrams Thermochem. 46 (2014) 62–79, https://doi.org/10.1016/j.calphad.2014.02.001.

[15] J. Drowart, P. Goldfinger, Investigation of inorganic systems at high temperature by mass spectrometry, Angew Chem. Int. Ed. Engl. 6 (7) (1967) 581–596, https://doi.org/10.1002/anie.196705811.

[16] M. Marezio, J.P. Remeika, Bond lengths in the α-Ga2O3 structure and the high-pressure phase of Ga2-xFexO3, J. Chem. Phys. 46 (5) (1967) 1862–1865.

[17] J. Åhman, G. Svensson, J. Albertsson, A reinvestigation of β-gallium oxide, Acta Crystallogr. Sect. C Cryst. Struct. Commun. C52 (1996) 1336–1338, https://doi.org/10.1107/S0108270195016404.

[18] N. Nadaud, et al., Structural studies of tin-doped indium oxide (ITO) and In4Sn3O12, J. Solid State Chem. 135 (1998) 140–148, https://doi.org/10.1006/jssc.1997.7613.

[19] J. Drowart, et al., High-temperature mass spectrometry: instrumental techniques, ionization cross-sections, pressure measurements, and thermodynamic data (IUPAC technical report), Pure Appl. Chem. 77 (4) (2005) 683–737, https://doi.org/10.1351/pac200577040683.

[20] C.I. Whitman, On the measurement of vapor pressures by effusion, J. Chem. Phys. 20 (1) (1952) 161–164, https://doi.org/10.1063/1.1700161.

[21] K. Motzfeldt, Ther thermal decomposition of sodium carbonate by the effusion method, J. Phys. Chem. 59 (2) (1955) 139–147.

[22] E.H. Copland, N.S. Jacobson, Measuring Thermodynamic Properties of Metals and Alloys, 2010, https://doi.org/10.1002/9781118180730.ch48. *NASA/TP-2010-216795*.

[23] R.P. Burns, Systematics of the evaporation coefficient Al2O3, Ga2O3, In2O3, J. Chem. Phys. 44 (1966) 3307–3319, https://doi.org/10.1063/1.1727229.

[24] D.W. Bonnell, J.W. Hastie, 'Program SIGMA'. Program SIGMA is available on request, together with σ vs. E coefficient data, in: IBM PC Executable Format or as Source Code, National Institute of Standards and Technology, Inithersburg, MD, 1990 (unpublished work).

[25] N.S. Jacobson, Mass spectrometric studies of oxides, ECS Trans. 46 (39) (2013), https://doi.org/10.1002/oms.1210060109.

[26] H. Deutsch, et al., The semiempirical deutsch-märk formalism. A versatile approach for the calculation of electron-impact ionization cross sections of atoms, molecules, ions, and clusters, Adv. Atom. Mol. Opt. Phys. 57 (2009) 87–155, https://doi.org/10.1016/S1049-250X(09)57003-6.

[27] R.S. Freund, et al., Cross-section measurements for electron-impact ionization of atoms, Phys. Rev. 41 (7) (1990) 3575–3595, https://doi.org/10.1103/PhysRevA.41.3575.

[28] Y.K. Kim, P.M. Stone, Ionization of boron, aluminum, gallium, and indium by electron impact, Physical Review A - Atomic, Molecular, and Optical Physics 64 (5) (2001) 11, https://doi.org/10.1103/PhysRevA.64.052707.

[29] D. Margreiter, H. Deutsch, T.D. Märk, A semiclassical approach to the calculation of electron impact ionization cross-sections of atoms: from hydrogen to uranium, Int. J. Mass Spectrom. Ion Process. 139 (1994) 127–139.

[30] C.J. Patton, et al., Multiple ionization of gallium by electron impact, J. Phys. B Atom. Mol. Opt. Phys. 29 (1996) 1409–1417.

[31] W. Lotz, Electron-impact ionization cross-sections for atoms up to Z=108, Z. Phys. 232 (1970) 101–107, https://doi.org/10.1007/BF01393132.

[32] W.L. Fite, R.T. Brackmann, Ionization of atomic oxygen on electron impact, Phys. Rev. 113 (3) (1959) 815–816, https://doi.org/10.1103/PhysRev.113.815.

[33] J.H. Gross, Mass Spectrometry - A Textbook, third ed., Springer, Berlin/Heidelberg, 2017 https://doi.org/10.1021/ac00269a027.

[34] S. Chapman, T.G. Cowling, The Mathematical Theory of Non-uniform Gases - an account of the kinetic theory of viscosity, thermal conduction, and diffusion in gases, in: Journal of Chemical Information and Modeling., 3rd ed., Cambridge University Press, Cambridge, UK, 1970.

[35] P. Atkins, J. de Paula, Physical Chemistry, tenth ed., W. H. Freeman and Company, New York, 2014 https://doi.org/10.1007/SpringerReference_77053.

[36] K. Nakajima, Determination of optimal vapor pressure data by the second and third law methods, Mass Spectrom. 5 (S0055) (2016) 1–6, https://doi.org/10.5702/massspectrometry.s0055.

[37] G.V. Chaplygin, No title, Zh. Fiz. Khim. 49 (1975) 2767–2771.

[38] V.A. Medvedev, et al., in: V.P. Glushko, U.S.S.R. Akad Nauk (Eds.), Thermicheskie Konstanty, Veshchestv (Thermal Constants of Substances), 1981 (Viniti, Moscow).

[39] J. Hultgren, et al., Selected Values of the Thermodynamic Properties of the Elements (A) and of the Binary Alloys (B), American Society for Metals, 1973.

[40] I. Barin, Thermochemical Data of Pure Substances, third ed., VCH, Weinheim, Germany, 1995.

[41] I.D. Petsalakis, et al., Theoretical ab initio study on the electronic states of GaO and Ga2O, J. Mol. Struct. 672 (2004) 105–111, https://doi.org/10.1016/j.theochem.2003.11.031.

[42] S. Mukhopadhyay, et al., Theoretical study of small clusters of indium oxide: InO, In2 O, InO2, In2 O2, J. Mol. Struct.: THEOCHEM 948 (2010) 31–35, https://doi.org/10.1016/j.theochem.2010.02.016.

[43] D.A.J. Lynch, Infrared Spectra of Group IIIA Metal Oxides, NASA-CR-133100, 1972.

[44] D.M. Makowiecki, D.A. Lynch, K.D. Carlson, No title, J. Phys. Chem. 76 (1971) 1963.

[45] E.H.P. Cordfunke, R.J.M. Konings, W. Ouweltjes, The standard enthalpy of formation of In_2O_3, J. Chem. Thermodyn. 23 (1991) 451–454.